AgRISTARS

SM-K2-04284

A Joint Program for Agriculture and Resources Inventory Surveys Through Aerospace Remote Sensing

Soil Moisture

April 1982

COMPUTER SIMULATION OF A SPACE SAR USING A RANGE-SEQUENTIAL PROCESSOR FOR SOIL MOISTURE MAPPING

Masaharu Fujita and Fawwaz Ulaby

Remote Sensing Laboratory
University of Kansas Center for Research, Inc.
2291 Irving Hill Drive - West Campus
Lawrence, Kansas 66045

Lyndon B. Johnson Space Center
Houston, Texas 77058

1. Report No.	2. Government Accession No.	3. Recipient's Catalog No.
SM-K2-04284		

4. Title and Subtitle	5. Report Date
COMPUTER SIMULATION OF A SPACE SAR USING A RANGE-SEQUENTIAL PROCESSOR FOR SOIL MOISTURE MAPPING	April 1982
	6. Performing Organization Code
7. Author(s)	8. Performing Organization Report No.
Masaharu Fujita and Fawwaz Ulaby	RSL TR 551-1
	10. Work Unit No.
9. Performing Organization Name and Address Remote Sensing Laboratory University of Kansas Center for Research, Inc. 2291 Irving Hill Drive - West Campus Lawrence, Kansas 66045	11. Contract or Grant No. NAS 9-16419
	13. Type of Report and Period Covered Technical Report
12. Sponsoring Agency Name and Address NATIONAL AERONAUTICS AND SPACE ADMINISTRATION Johnson Space Center Houston, Texas 77058	14. Sponsoring Agency Code

15. Supplementary Notes

16. Abstract In this report, the ability of a spaceborne synthetic-aperture radar (SAR) to detect soil moisture is evaluated by means of a computer simulation technique. The computer simulation package includes coherent processing of the SAR data using a range-sequential processor, which can be set up through hardware implementations, thereby reducing the amount of telemetry involved. With such a processing approach, it is possible to monitor the earth's surface on a continuous basis, since data-storage requirements can be easily met through the use of currently available technology.

The development of the simulation package is described first, followed by an examination of the application of the technique to actual environments. The results indicate that in estimating soil-moisture content with a four-look processor, the difference between the assumed and estimated values of soil moisture is within ±20% of field capacity for 62% of the pixels for agricultural terrain and for 53% of the pixels for hilly terrain. The estimation accuracy for soil moisture may be improved by reducing the effect of fading through non-coherent averaging.

17. Key Words (Suggested by Author(s))	18. Distribution Statement
Soil moisture mapping, radar remote sensing, SAR processing	

19. Security Classif. (of this report)	20. Security Classif. (of this page)	21. No. of Pages	22. Price*
U	U	105	

*For sale by the National Technical Information Service, Springfield, Virginia 22161

Remote Sensing Laboratory

The University of Kansas Center for Research, Inc.
2291 Irving Hill Drive-Campus West, Lawrence, Kansas 66045

Telephone: (913) 864-4832

COMPUTER SIMULATION OF A SPACE SAR USING A RANGE-SEQUENTIAL PROCESSOR FOR SOIL MOISTURE MAPPING

Remote Sensing Laboratory
RSL Technical Report 551-1

M. Fujita
F. T. Ulaby

April 1982

Fawwaz T. Ulaby, Principal Investigator

Supported by
NATIONAL AERONAUTICS AND SPACE ADMINISTRATION
Johnson Space Center
Houston, Texas 77058
CONTRACT NAS-9-16419

TABLE OF CONTENTS

ACKNOWLEDGMENTS

This research was supported by the National Aeronautics and Space Administration, Johnson Space Center, Houston, Texas 77058.

LIST OF FIGURES

LIST OF TABLES

ABSTRACT

In this report, the ability of a spaceborne synthetic-aperture radar (SAR) to detect soil moisture is evaluated by means of a computer simulation technique. The computer simulation package includes coherent processing of the SAR data using a range-sequential processor, which can be set up through hardware implementations, thereby reducing the amount of telemetry involved. With such a processing approach, it is possible to monitor the earth's surface on a continuous basis, since data-storage requirements can be easily met through the use of currently available technology.

The development of the simulation package is described first, followed by an examination of the application of the technique to actual environments. The results indicate that in estimating soil-moisture content with a four-look processor, the difference between the assumed and estimated values of soil moisture is within ±20% of field capacity for 62% of the pixels for agricultural terrain and for 53% of the pixels for hilly terrain. The estimation accuracy for soil moisture may be improved by reducing the effect of fading through noncoherent averaging.

This Page Intentionally Left Blank

1.0 INTRODUCTION

Although the synthetic aperture radar (SAR) that was carried aboard Seasat-A in 1978 was configured as an ocean-monitoring sensor, the images of land surfaces it produced have provided valuable information for a variety of applications including geology, land use, and soil-moisture detection. The Seasat-A SAR results, together with those recently obtained from Shuttle SAR imagery, have generated momentum in the remote sensing community for increased support and emphasis on the utilization of imaging radar for earth observations.

One of the applications for which radar imagery is particularly suitable is soil moisture mapping. The availability of information concerning the temporal and spatial variations of soil moisture can be extremely valuable for hydrologic, agricultural, and meteorological applications. The radar response to soil moisture has been investigated in several studies over the past decade and optimum sensor parameters have been defined (Ulaby et al., 1978, 1979; Dobson and Ulaby, 1981). The results of these studies are based on experimental measurements conducted from truck-mounted and airborne platforms. To examine the performance of a space-SAR soil-moisture sensor, a computer simulation study was conducted using data from a test site containing an agricultural floodplain as well as hilly terrain (Ulaby et al., 1981). A soil moisture simulation study also was conducted by Meier (1981) for a real-aperture radar (RAR).

In the previous SAR simulations (Ulaby et al., 1981), the spatial resolution and the number of looks were specified and variations due to signal fading were computed based on Rayleigh statistics. However, the

effects of the synthesized aperture were not taken into account. This report examines sidelobe effects as viewed by computer simulation of a SAR using a range-sequential processor. This type of processor, which was chosen because of its capability to process data aboard a satellite (thereby reducing the amount of telemetry needed), was proposed by Moore et al. (1977) for mapping different types of sea ice.

2.0 SAR MODEL

2.1 General Description

SARs may be divided into different classes on the basis of the scheme used to process successive echoes. These differences pertain to only the azimuth (along-track) resolution.

Among the various SAR-processing schemes, we have adopted a range-sequential approach (Moore et al., 1977) in order to simulate SAR processing because of its potential to reduce the amount of telemetry data, which may be an advantage for the continuous monitoring of soil moisture by a spaceborne SAR since, in the range-sequential processor, coherent processing of the echoes is accomplished in real time by means of analog circuitry onboard the satellite. In almost all of the other approaches, coherent processing is done after collecting and storing the echoes, which may require large amounts of computer-processing time.

The following description of the range-sequential processor is based on a report by Moore et al. (1977). Figure 1 shows a block diagram of a comb-filter, which is a key element in the makeup of the range-sequential processor. In the figure, T_p refers to the amount of time delay which is chosen to be the same as the interpulse period. The interpulse period must be an integer number of cycles at the carrier frequency.

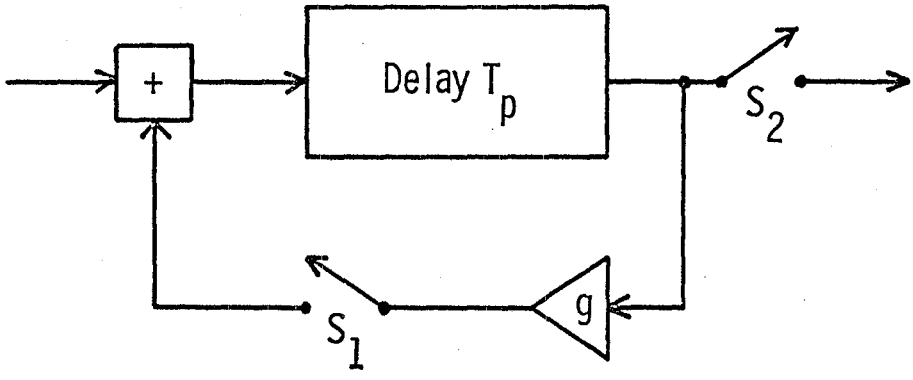

Fig. 1. Implementation of the comb-filter.

In the first stage, switch S_1 is closed and S_2 is open. After the first echo passes through the delay element, the signal is fed back toward the input of the delay element. Since the amount of delay is exactly the same as the interpulse period and the interpulse period is an integer number of cycles at the carrier frequency, the delayed signal is added in phase to the second echo. The summed signal again passes through the delay element and is added to the third echo and so on. This in-phase addition, which corresponds to the coherent along-track processing, can be done along the across-track direction before range sampling -- thus the name "range sequential processor." After the addition of the necessary number of echoes, S_1 is opened and S_2 is closed to allow the output of the comb-filter to be processed. The output of the filter consists of processed images of the target in the along-track direction and in the range-sequential manner. By sampling the output with an appropriate range interval, we can obtain the images of the target in the across-track direction. The feedback gain g in the figure can taper with aperture distribution along the synthesized array to control the sidelobe level and the beamwidth. In the present study, however, no aperture taper is introduced because of the complexity of calibrating a SAR as a scatterometer. A relatively high sidelobe level may, therefore, degrade the SAR's capability for fine-resolution along-track mapping of the target.

To use the comb-filter as a SAR processor, a bank of filters is necessary to map the target two-dimensionally. The discrimination of the target in the along-track direction is made by using the difference in the Doppler frequency. The Doppler frequency shifts of targets at

different locations, for a sidelooking radar are illustrated in Fig. 2. Each trace represents the history of the Doppler shift for a target located at a different position along the spacecraft's trajectory. By applying an appropriate phase correction to the radar echo to eliminate the phase rotation due to the Doppler shift, the history of each target echo represented by a solid line in Fig. 2 is translated into a constant frequency bias as shown in Fig. 3. Appropriate conversions of frequency allow us to extract the specific frequency component that corresponds to the image of the specific target produced by the comb-filter.

For the following simulations, the SAR is assumed to have the form shown in Fig. 4 in order to map the target area two-dimensionally. The Doppler frequency shift is compensated for by the sweep oscillator in the figure. After that, the echo from each particular target has a constant frequency deviation from the radar frequency. Signals from the offset frequency synthesizer are applied to each echo to extract the specific frequency component by the band of comb-filter.

2.2 Design of the SAR for Simulation

For computer simulations, some parameters of the SAR must be determined by referring to the aim of the work. Since the final goal of the present study is to evaluate the ability of a SAR to detect soil moisture, the frequency of the radar should be chosen to be between 4 GHz and 5 GHz as recommended by Ulaby et al. (1981). For ease of comparison with the previous simulation results and due to the availability of experimental data relating the backscattering coefficient and the soil moisture, the frequency chosen is 4.75 GHz with horizontal polarization

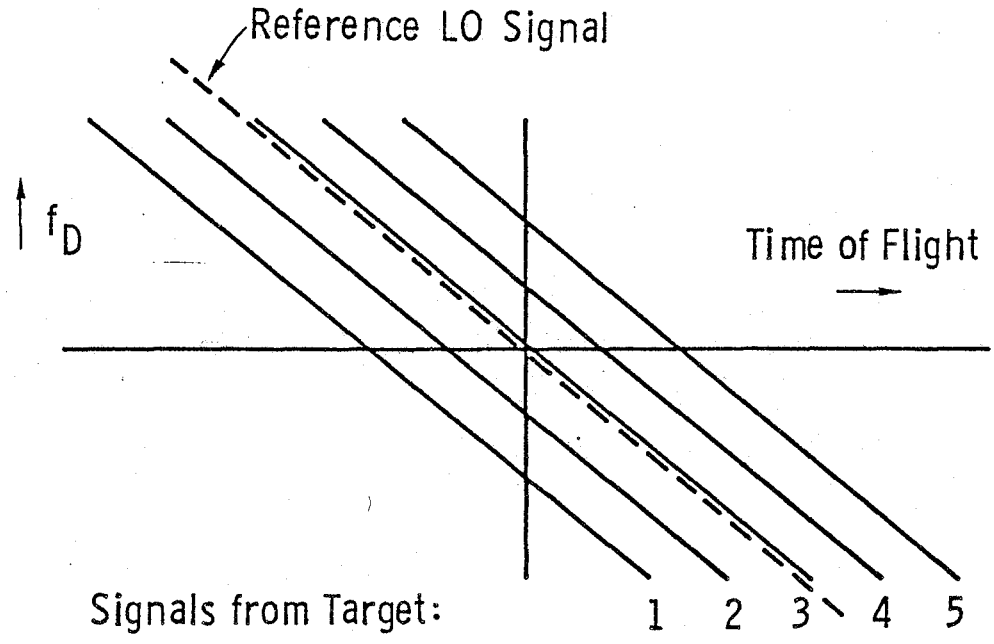

Fig. 2. Histories of the Doppler frequency shift for five targets (after Ulaby et al., 1982).

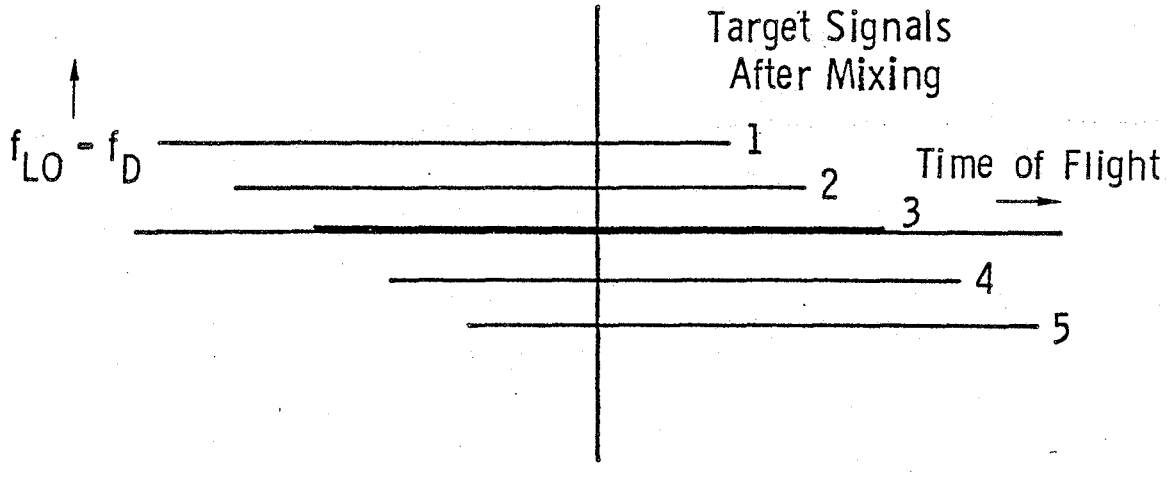

Fig. 3. Histories of the Doppler frequency shift for five targets after frequency compensation (after Ulaby et al., 1982).

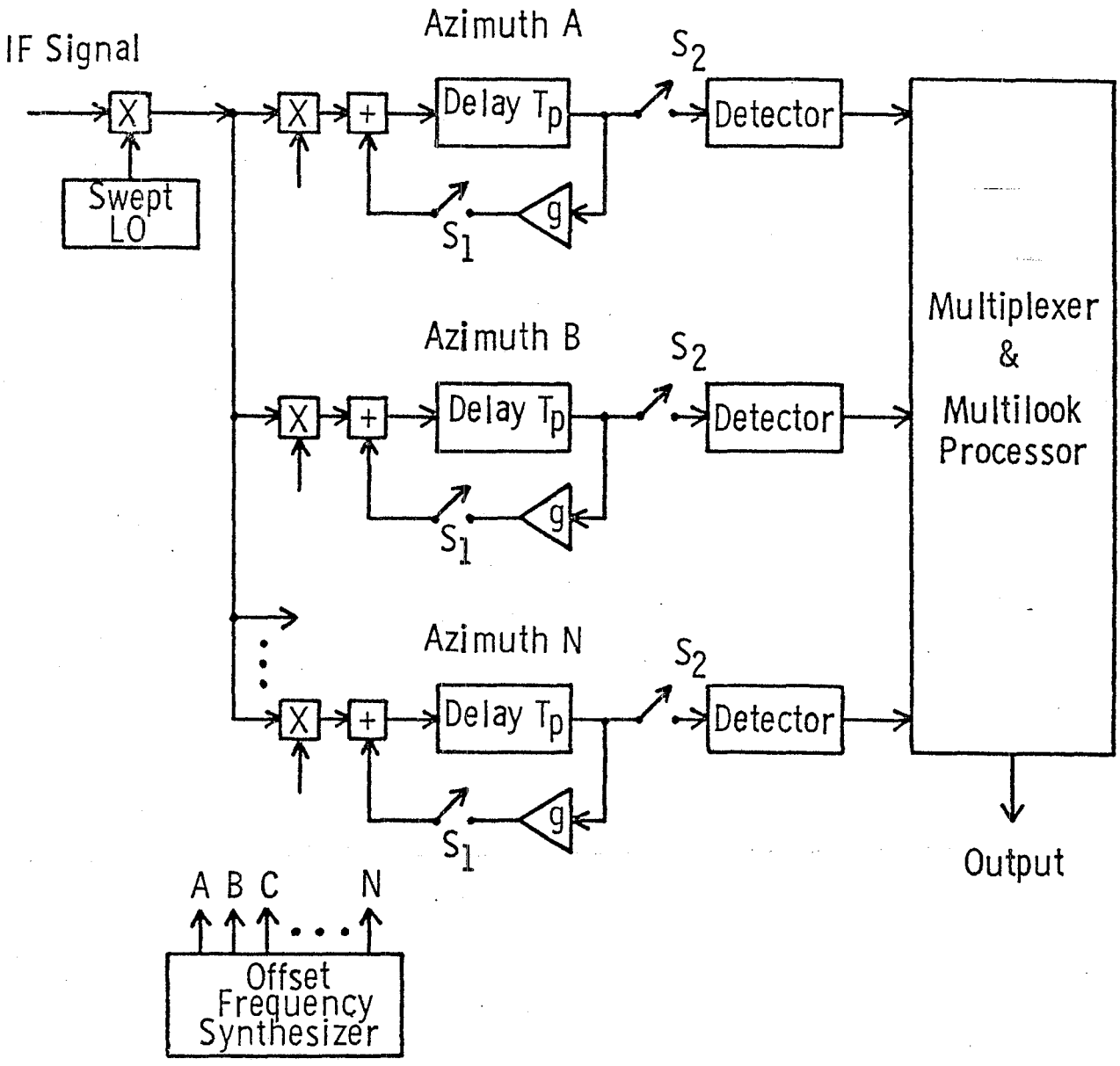

Fig. 4. Block diagram of the range-sequential processor model in the simulation (after Ulaby et al., 1982).

for transmission and reception. As stated later, the target area is very small (1.8 km x 1.8 km), therefore, for simplicity of treatment, the earth is assumed to be flat. However, considerations for determining the parameters of the SAR are also made for the earth as a sphere in terms of actual application.

For a SAR being carried by a spacecraft at an altitude of 600 km, the slant-swathwidth is 38.5 km for the range of incidence-angle between 7 degrees and 22 degrees as shown in Fig. 5 (Ulaby et al., 1981). The pulse-repetition frequency f_p must be chosen so that the echoes from the swathwidth do not overlap each other for two successive pulses. Therefore,

$$f_p \leqq C/2R_s = 3896.1 \text{ (Hz)}, \tag{1}$$

where c is the velocity of light and R_s is the slant swathwidth.

Additionally, f_p must satisfy the following equation to obtain the Doppler frequency-shift components that are necessary for a range sequential processor:

$$f_p \geqq 4u/L, \tag{2}$$

where u is the speed of the spacecraft carrying the SAR and L is the antenna length of the SAR along its direction of motion. The speed of the spacecraft, at an altitude of 600 km, is calculated to be 7545 m/sec and the antenna length is chosen as 8.7 m, in accordance with the previous work, so that Eq. 2 becomes,

$$f_p \geqq 3469.0 \text{ (Hz)}. \tag{3}$$

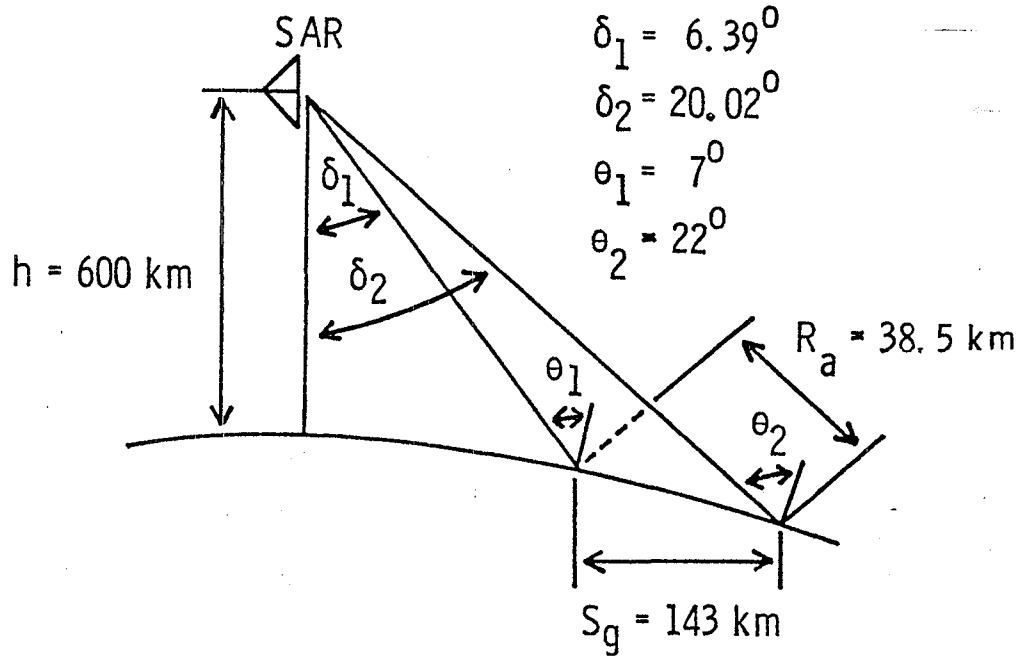

Fig. 5. Geometry of a side-looking radar at an altitude of 600 km for a spherical earth (after Ulaby et al., 1981).

Since the radar frequency must be an integer multiple of the pulse-repetition frequency in the range-sequential processor, the pulse-repetition frequency f_p and the radar frequency f were chosen to be 3600 Hz and 4.750002 GHz, respectively.

The maximum obtainable resolution of a SAR with an antenna length of 8.7 m is 4.35 m; one half of the antenna length, according to theory (Ulaby et al., 1982). However, due to the limitations of computer memory and computer time, an along-track resolution for a one-look processor is assumed to be 36 meters.

The data base to be mapped by the SAR is now assumed to be a 1.8-km x 1.8-km-square area with the angle of incidence to the center being 7.5 degrees as shown in Fig. 6. The length from the SAR to the data-base center R_o is 605.177 km.

The length of the synthetic aperture L_{ap} and the resolution in the along-track direction r_a are related approximately as follows:

$$L_{ap} = \frac{R_o \lambda}{r_a} , \tag{4}$$

where λ is the wavelength of the radar frequency. By substituting R_o = 605.177 km, λ = 6.316 cm, and r_a = 36 m, the length of the synthetic aperture needed to realize a 36-meter resolution can be calculated as L_{ap} = 1061.7 meters. The necessary number of pulses is then obtained as follows:

$$f_p \times L_{ap}/u + 1 \cong 508. \tag{5}$$

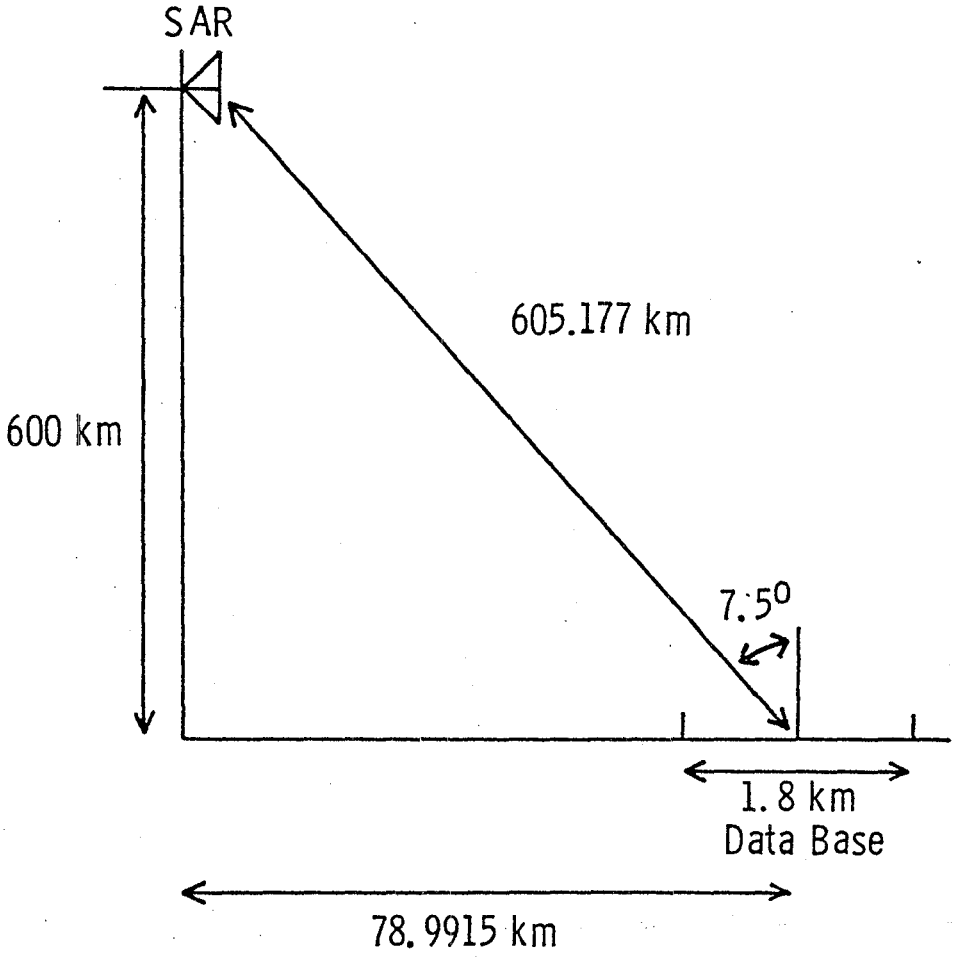

Fig. 6. Geometry of the SAR and the data base.

In a partially focused SAR, fine along-track resolution can be achieved by discriminating the target using the differences in Doppler frequency shifts. As for the range-sequential processor, frequency offsets are applied to the video signal to shift the spectrum. Then the appropriate frequency component is extracted by the following comb-filter. The amount of the Doppler frequency shift, which could be compensated for by the frequency offsetting corresponding to the length of one resolution cell is expressed by,

$$\frac{2ur_a}{\lambda R_o} \cong 14.2 \text{ (Hz)} . \tag{6}$$

Therefore, coherent-reference oscillators with frequencies differing by a shift of 14.2 Hz must be used, the number of which is equal to the number of along-track resolution cells. In the present case, a 36-meter resolution is assumed for a data-base length of 1.8 km, so that the number of coherent oscillators is 50.

In the partially focused SAR, depth of focus should be considered; however, it can be ignored in the present case because of the short swathwidth of the assumed data base.

It is assumed that the across-track resolution becomes 36 meters after range sampling. The receiver bandwidth is sufficiently wide for the transient of the range-sampling signal to die out quickly and not affect the following samples.

3.0 COMPUTER SIMULATIONS FOR CONTROLLED SCENES

3.1 Brief Explanation of the Simulations

The simulation program begins with the transmitted pulse. The pulse-repetition frequency is 3600 Hz and the number of pulses needed is 508, so that the actual time for mapping the data base is,

$$(508-1)/3600 \cong 0.141 \text{ (sec)}. \tag{7}$$

However, much more time is necessary for computer simulations. The first pulse is transmitted when the SAR is located at a distance of -531.3 m from the center coordinate of the data base, and the 508th (last) pulse is transmitted at 531.3 m from the center coordinate in the along-track direction as shown in Fig. 7. The echoes from each data-base cell are calculated for the received power and its phase angle by accounting for the round-trip distance traveled by the pulses. No phase rotation is assumed in the scattering process. The received echoes are then divided into so-called in-phase and quadrature components and accumulated into the appropriate range-bin memory. In the actual range-sequential processor in which hardware implementations are employed, range sampling will be made after accumulating the echoes in analog form. In the computer simulations, however, all data have to be handled in a discrete form, so that range sampling is made first, before the data accumulations. These calculations are made for each transmitted pulse across the entire data base. The number of echo calculations per single transmitted pulse is 50 x 50 = 2500 and the number of transmitted pulses is 508, so that the total number of echo calculations is 1,270,000.

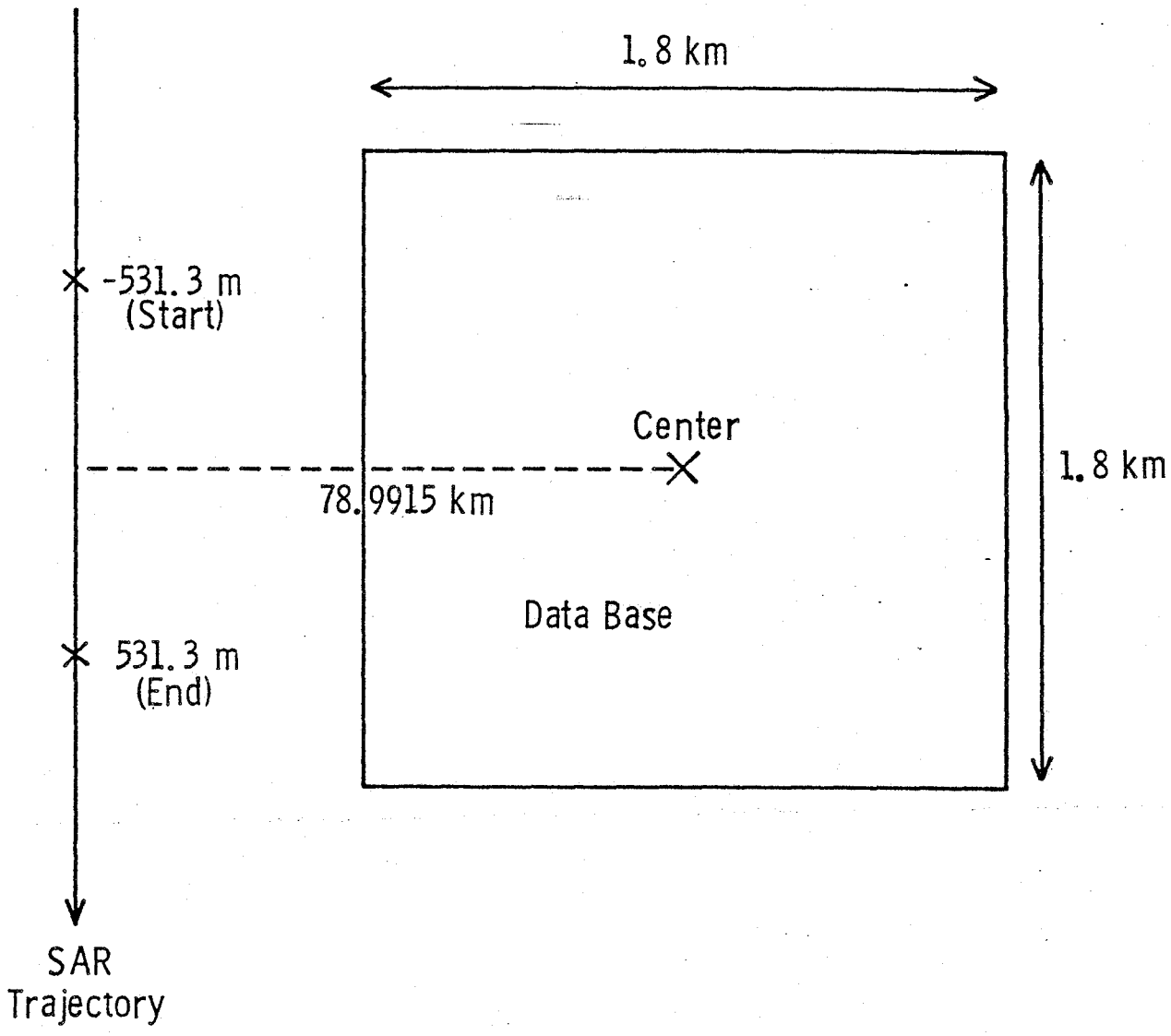

Fig. 7. SAR dimensions and data base.

After completing the calculations, the contents of the two-dimensional computer memory are examined to obtain a two-dimensional map of the data base. The output of each of the 50 comb-filters provides a map of a 36-meter-wide strip in the along-track direction, and range sampling provides a 36-meter resolution in the across-track direction on the flat surface.

3.2 Flat Earth

At the beginning of the work, a simplified data base is assumed, in which a square, a triangle, a cross, and a hexagon are included as shown in Fig. 8. The data base is 1.8 km x 1.8 km, with cells of 36 m x 36 m on a flat earth. There is no elevation variation across the data base. The backscattering coefficient σ^{o} is assumed to be 10 m^2/m^2 inside the four figures (symbol "a" areas) and 0 outside them. For the geometrical relationship between the SAR and the data base, refer to Figs. 6 and 7. In the simulations, the distance term in the radar equation is fixed at a constant value, since the distances to the farthest and nearest targets are approximately the same and the difference between them is very small compared with the distances themselves.

Figure 9 shows the results of simulation for the data base of Fig. 8. Each number in the figure represents a resolution cell of 36 m x 36 m and its value is the estimated backscattering coefficient obtained at each resolution cell. The range of the backscattering coefficients and their numbers are listed in Table 1 to relate them to each other. In accordance with the assumption, the backscattering coefficients inside the figures should be 10; however, almost all of the estimated backscattering coefficients are smaller than 10. This may

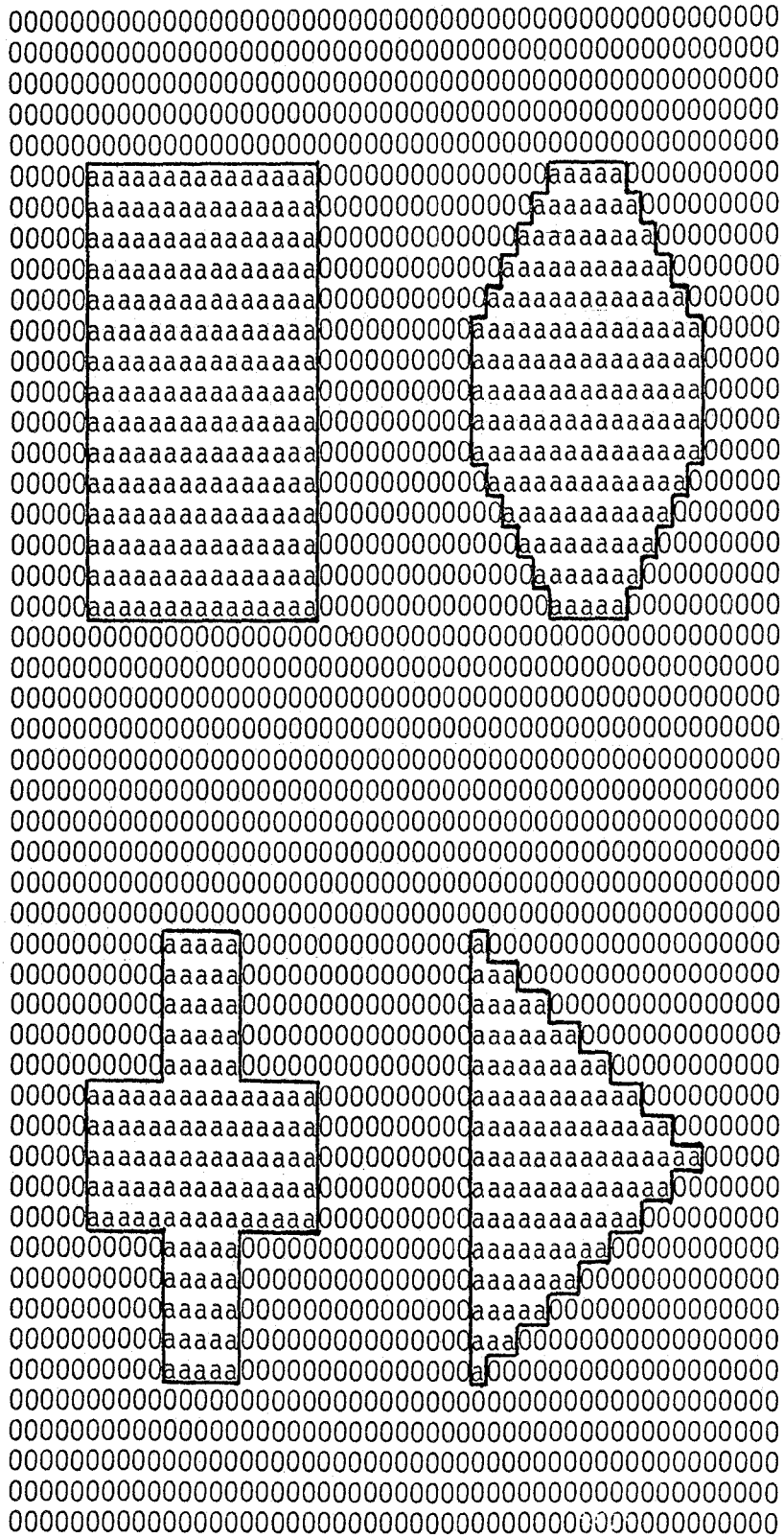

Fig. 8. Assumed Target Area 1.

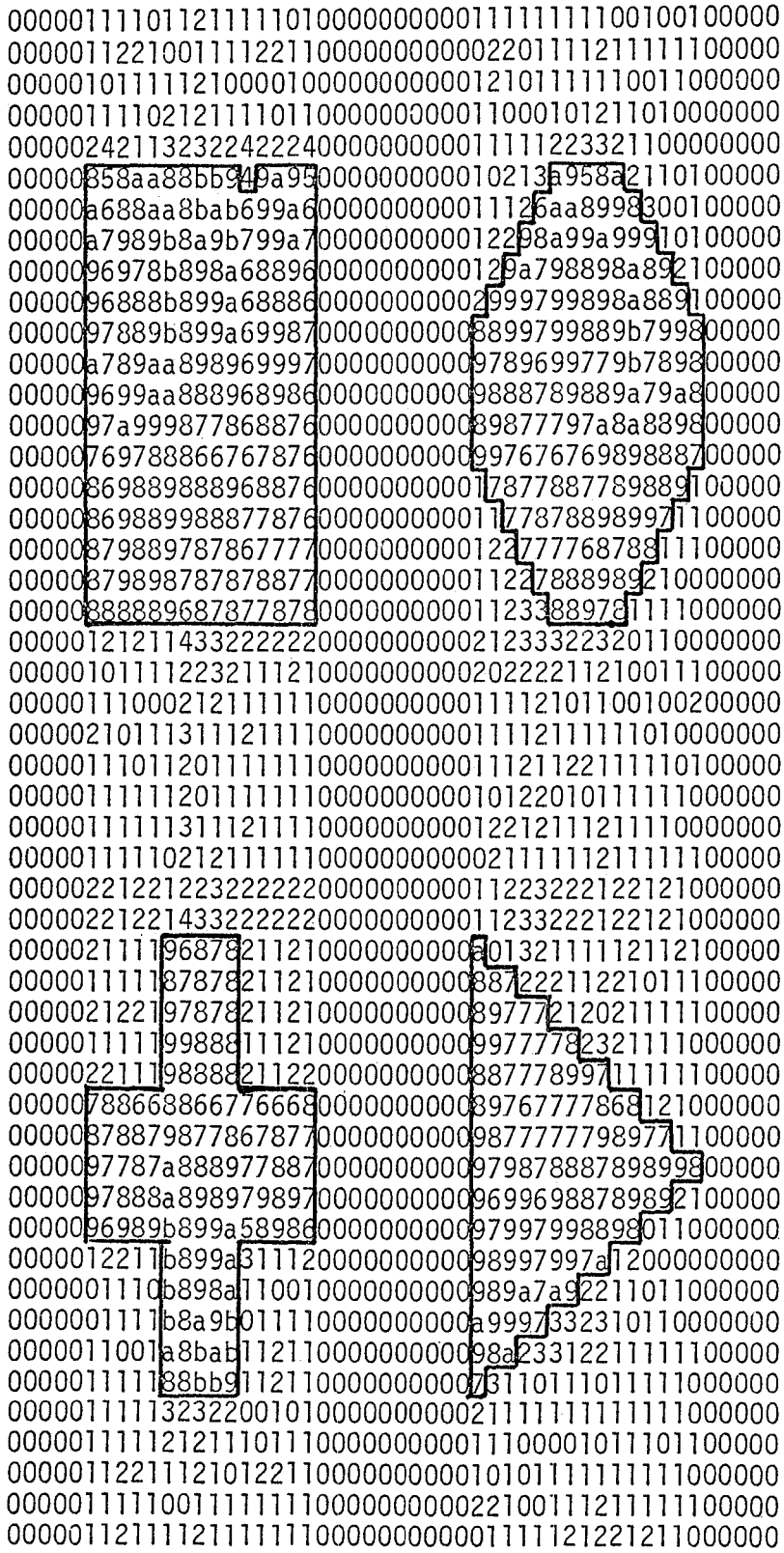

Fig. 9. Image of Target Area 1.

TABLE 1

Correspondence Between the Symbols that Appear in the Simulation Image and the Backscattering Coefficient in Real Value

Letter or Number	Range of Scattering Coefficient
0	$0 \leqslant, < 0.5$
1	$0.5 \leqslant, < 1.5$
2	$1.5 \leqslant, < 2.5$
3	$2.5 \leqslant, < 3.5$
4	$3.5 \leqslant, < 4.5$
5	$4.5 \leqslant, < 5.5$
6	$5.5 \leqslant, < 6.5$
7	$6.5 \leqslant, < 7.5$
8	$7.5 \leqslant, < 8.5$
9	$8.5 \leqslant, < 9.5$
a	$9.5 \leqslant, < 10.5$
b	$10.5 \leqslant, < 11.5$
c	$11.5 \leqslant, < 12.5$
d	$12.5 \leqslant, < 13.5$
e	$13.5 \leqslant, < 14.5$
f	$14.5 \leqslant, < 15.5$

be the result of coherency between received echoes. In the present simulation, no illumination taper is applied along the synthetic aperture, so that the sidelobes are relatively high compared with the usual antenna-array system. The echoes picked up by these relatively high sidelobes may affect the coherency between the echoes.

The radiation pattern of the synthetic array is written as follows:

$$F(\phi) = \frac{\sin(254\phi)}{\sin\frac{\phi}{2}} \tag{8}$$

with

$$\phi = \frac{2\pi d}{\lambda}\sin\theta \tag{9}$$

where θ is the angle measured from boresight and d is the distance between the array elements, which corresponds to the distance the SAR travels during the one-pulse interval. Therefore d is given as,

$$d = \frac{7545}{3600} = 2.096 \text{ (m)}, \tag{10}$$

λ is the wavelength of the radar signal and equal to 6.316×10^{-2} m. In this case, the first sidelobe peak may occur in the vicinity of $254\phi = 270$ (degrees) and its level is computed to be about -13.5 dB relative to the mainbeam. By solving Eq. 9, substituting the values of d and λ, and approximating $\sin\theta \cong \theta$, the first sidelobe occurs at the angle of 8.9×10^{-5} radians from the mainlobe. This means that, at a distance of 605 km, the first sidelobe points to the location 53.8 meters away from the mainlobe location. The echoes in the first sidelobe direction are -27 dB relative to those in the mainbeam direction

because of two-way attenuation. This value can be further reduced by applying the aperture taper along the synthetic array; however, for simplicity of the treatment, no aperture taper is adopted in the present simulations.

Interpretation of the underestimated backscattering coefficients will be made later.

3.3 Flat Earth with Elevation Variations

In the previous simulation, the data base was assumed to be perfectly flat, meaning that there are no elevation variations. The effects of overlay and shadow, therefore, do not appear in the simulation results. In the actual environment, however, there are elevation variations, such as hills, mountains, and valleys, so that it is necessary to develop a simulation package that can handle a target area having elevation variations. The modification to the previous simulation package is to select the appropriate range-bin memory for each echo according to the distance between the SAR and each of the data-base cells.

Figure 10 shows a distribution of the backscattering coefficients across the data base to be mapped in the simulation. In the figure, "a" means that the backscattering coefficient is 10 m^2/m^2. In Fig. 11, the elevation variations are shown for the data base as it is seen from above and along the spacecraft trajectory. The height of the hill and the depth of the valley are 50 meters and the height of the tower located at the very center of the data base is 100 meters.

Computer simulation is made for the data base and the results are shown in Fig. 12. Again each number represents a 36-m x 36-m resolution cell and the value refers to the scattering coefficient as listed in

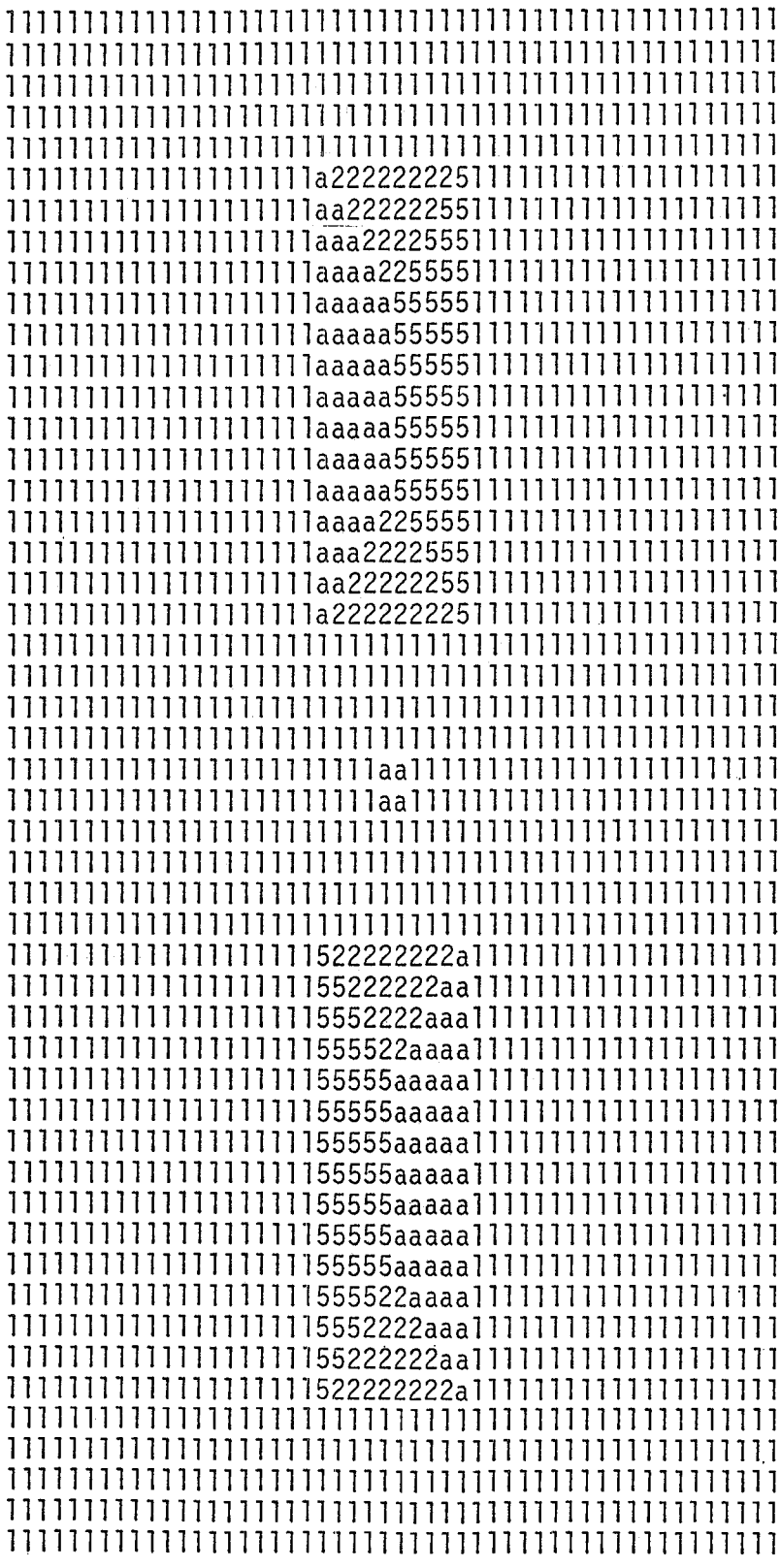

Fig. 10. Assumed Target Area 2.

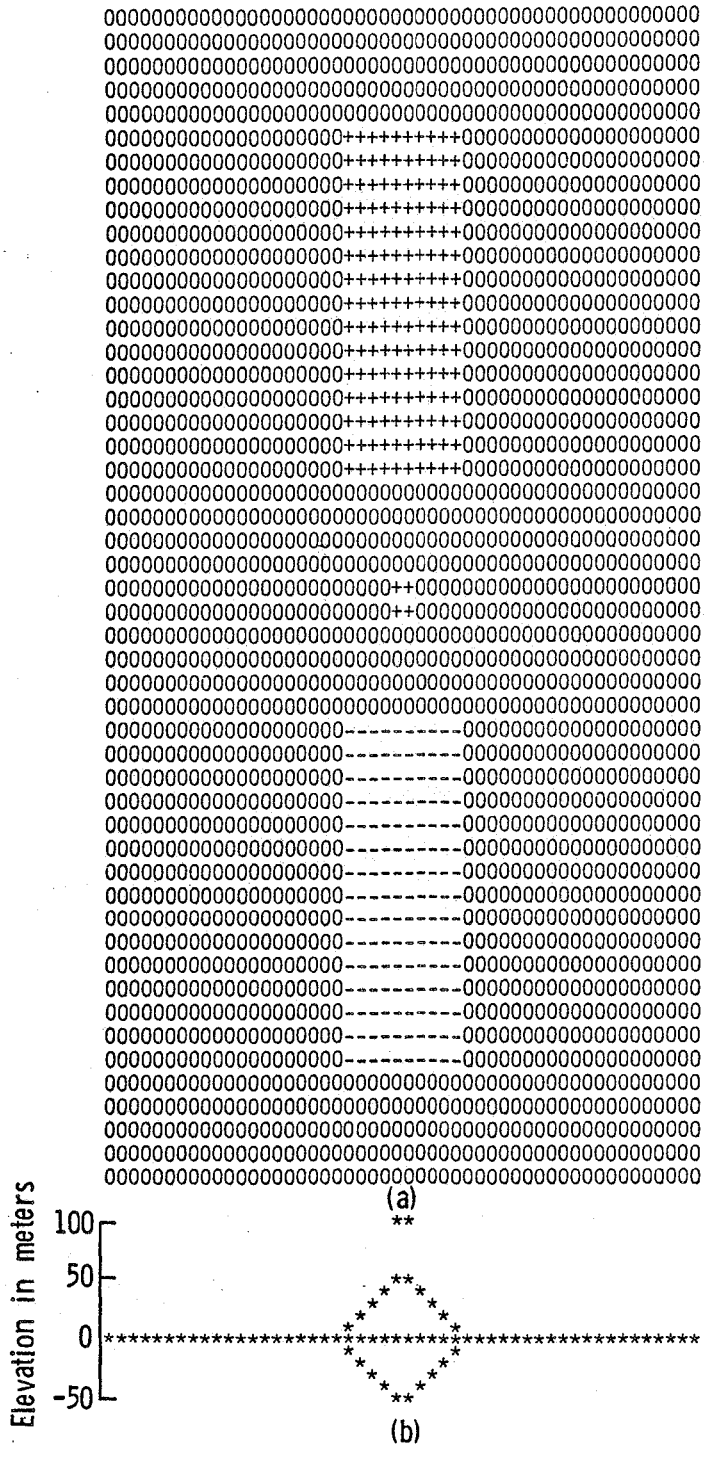

Fig. 11. Distribution of the elevation variation of Target Area 2: (a) as seen from upside + and - mean high and low places, respectively, and (b) as seen from the side.

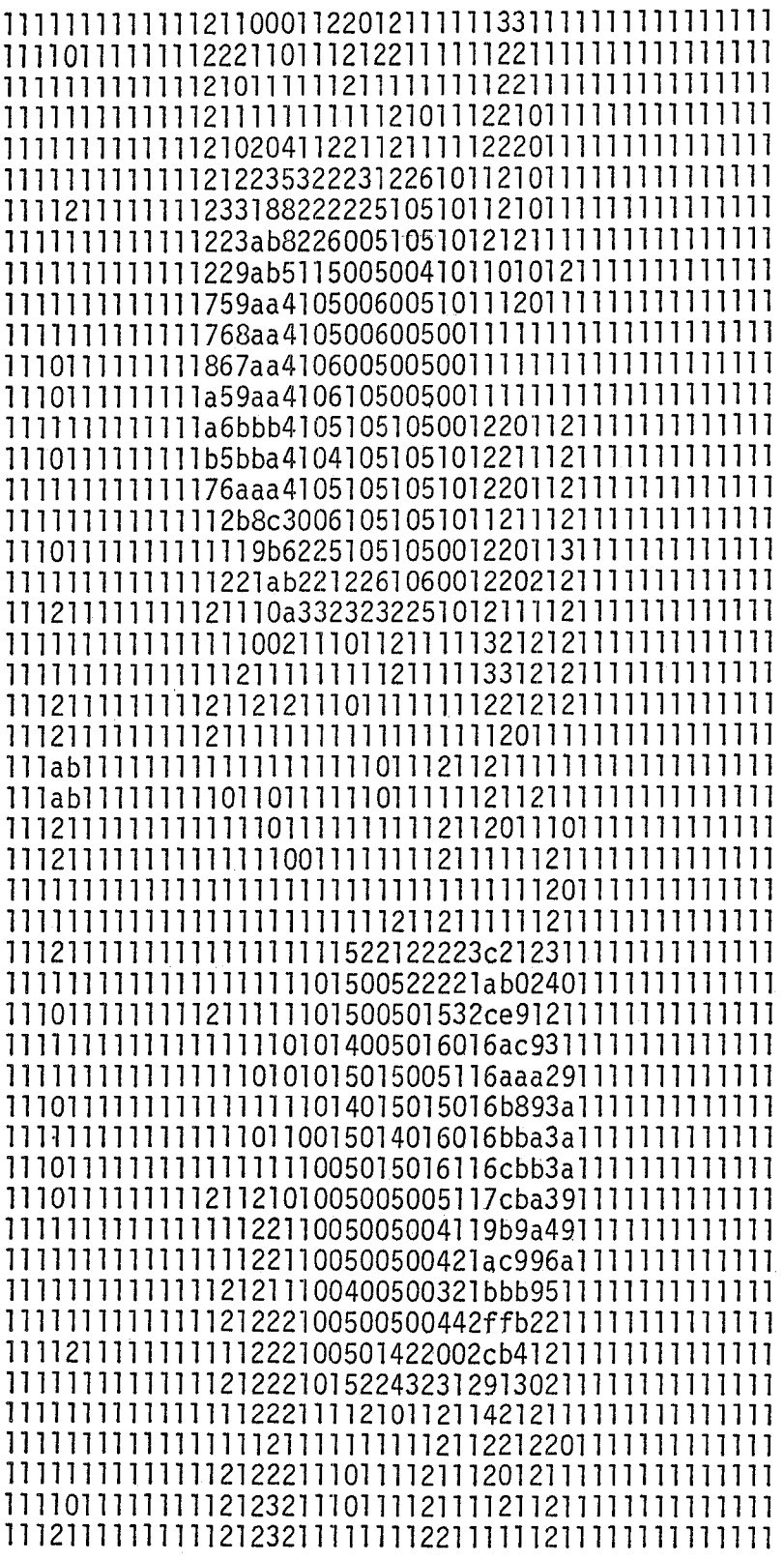

Fig. 12. Image of Target Area 2.

Table 1. All of the SAR parameters are the same as those in the previous simulation. The incidence angle to the flat earth is designed to be 7.5 degrees, so that the effect of the shadow of the image cannot actually be seen except for the tall tower at the center. Since the slopes of the hill and the valley are not steeper than the angle of incidence, there are no shadows in the other regions.

On the other hand, the effect of overlay can be clearly seen in Fig. 12, which demonstrates the advantage of using the present simulation package. The estimated backscattering coefficients also differ slightly from the assumed values in the data base of the previous simulation. The countermeasure against this tendency is discussed in the next section.

3.4 Calibration of the SAR

In scatterometer measurements, the scattering coefficients are estimated by solving the radar equation along with the measured received power. Therefore, calibration of the scatterometer becomes significant for accurate measurements of the backscattering coefficients. Usually, a kind of lens, or a metallic body having a known backscattering cross-section is employed for calibrating the scatterometer.

In a SAR, the received power at each resolution cell is obtained by coherent addition of echoes of a certain number of transmitted pulses, N. Therefore, the SAR's received power theoretically becomes N^2 times the received power for one trasmitted pulse. However, some causes, for example the sidelobe effect, may degrade coherency among the echoes, which results in the difference between the estimated and the assumed backscattering coefficients. To establish the relationship between the

estimated and the assumed backscattering coefficients, these quantities are compared with each other. These are chosen from among the results of the simulations described in the previous sections. The regions chosen for comparison are inside the four figures in Fig. 9 and in the upper-right and lower-left corners of Fig. 12.

Figure 13 shows the distributions of the echo amplitudes at each resolution cell for the specific areas. The upper one is the result for the square in Fig. 9 and the lower one is that for the upper right-hand corner in Fig. 12; the number of resolution cells in both examples is 225. In spite of the differences in the conditions of the surrounding backscattering coefficients, the shapes of the distributions are almost the same, and the difference in the averaged value is only 0.49 dB. In Table 2, the averaged values and the standard deviations of the echo amplitudes obtained by the previous simulations are shown, which are normalized by the theoretically derived amplitude of the resolution cells. From the above result, we will adopt a calibration factor of 0.825. This means that the measured amplitude is smaller than the theoretical value by an amount of -1.671 dB on the average. Therefore, we must add 1.671 dB to the simulated amplitude to account for the effect of side-lobe and other causes of errors in the computations. It should be noted that this compensation value is valid only for the present simulations, and different values may be adopted for SAR simulations with different parameters.

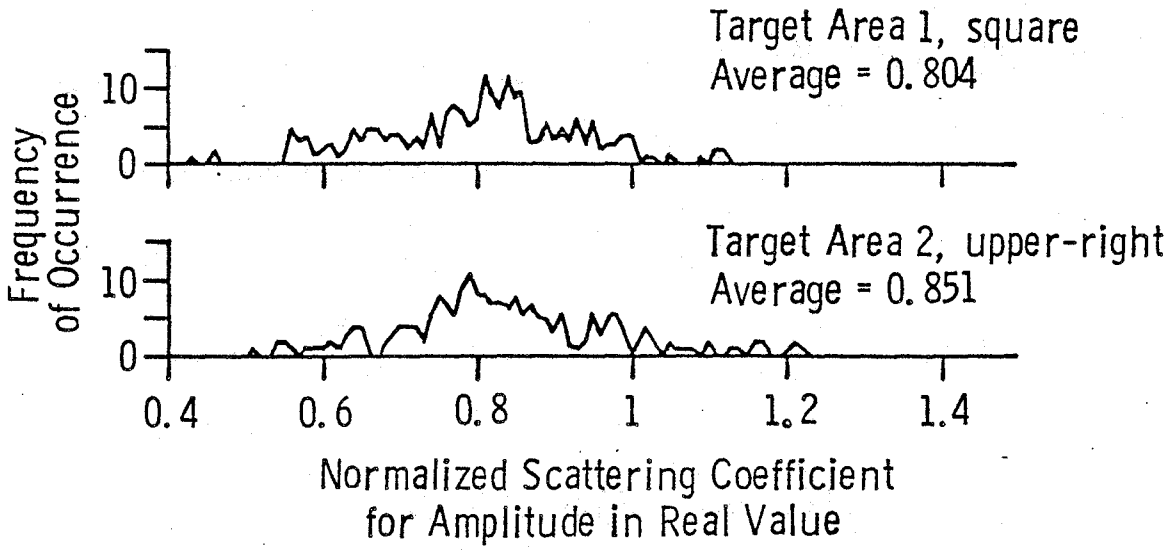

Fig. 13. Distributions of the estimated backscattering coefficient normalized by the assumed value.

TABLE 2

Summary of the Distributions of the Estimated Backscattering Coefficient Normalized by the Assumed Value

Target Area	Figure or Location	Averaged Backscattering Coefficient	Standard Deviation	Number of Samples
1	Square	0.804	0.132	225
1	Hexagon	0.824	0.103	165
1	Cross	0.817	0.125	125
1	Triangle	0.807	0.098	113
2	Upper Right	0.851	0.137	225
2	Lower Left	0.837	0.176	225
	Total Average:	0.825	Total Number of Samples:	1078

4.0 COMPUTER SIMULATIONS FOR SOIL MOISTURE ESTIMATION

4.1 General Description

The backscattering coefficients of soil both with and without vegetation cover vary according to soil water content. This means that, by measuring the backscattering coefficient of the soil, one can estimate its water content. Simulation studies for estimating soil moisture by means of a SAR (Ulaby et al., 1981) and a SLAR (Meier, 1981) have been made, the former being based on measurements of backscattering coefficients (Ulaby et al., 1978, 1979; Dobson et al., 1981). The SAR simulation, however, assumed a nominal resolution which may be attained by coherent processing.

The present section concerns a SAR simulation for soil moisture estimation in which the coherent processing of echoes is included in its entirety. The basic concept of the SAR simulation package is written and tested as described in the previous chapters, along with its calibration scheme.

4.2 Data Base

In evaluating the ability of a SAR to estimate soil moisture, two data bases are extracted from the large data base constructed for the previous work, whose test site was located east of Lawrence, Kansas (Ulaby et al., 1981). One of the data bases represents an almost flat area, which will be called the "floodplain" hereafter, and the other is a hilly area called "hilly" hereafter. These areas are chosen in order to compare the influence of surface elevation on

the accuracy of the soil moisture estimation. Both of the data bases again have dimensions of 1.8 km x 1.8 km, with cells of 36 m x 36 m, so that the number of cells is 2500.

The data base includes surface elevation, target category (i.e., bare soil, classes of vegetation, or cultural features) and soil texture. One can ignore the effect of soil texture when soil moisture is expressed by the percent of field capacity, M_{FC}, where field capacity is the gravimetric moisture content at 1/3-bar tension. In the following, therefore, we use only surface-elevation and target-category data. Figure 14 shows distributions of the target category across the floodplain and hilly data bases. Each letter represents the 36-m x 36-m cell and the letters S, V, T, W, and A correspond to the target categories of bare soil, vegetation-covered soil, trees, water bodies, and artificial objects, respectively. The bare soil category is divided into three groups according to surface roughness as shown in Table 3. The vegetation-covered soil is also divided according to the kind of vegetation present, as shown in Table 4. The soil moisture can be defined for the above two category groups; however, for trees, water bodies, and artificial objects, one cannot define the level of soil moisture. In Table 5, percentages of each target category are summarized for both data bases. The areas where soil moisture can be defined are 82.4% for the entire floodplain data base and 94.8% for the hilly area.

Figure 15 shows elevation distributions across the data bases; a plus (+) signifies that the elevation is higher than the reference elevation, and a minus (-) means the elevation is lower. The reference elevations are 246.9 m (810 ft.) for the floodplain and 265.2 m (870 ft.)

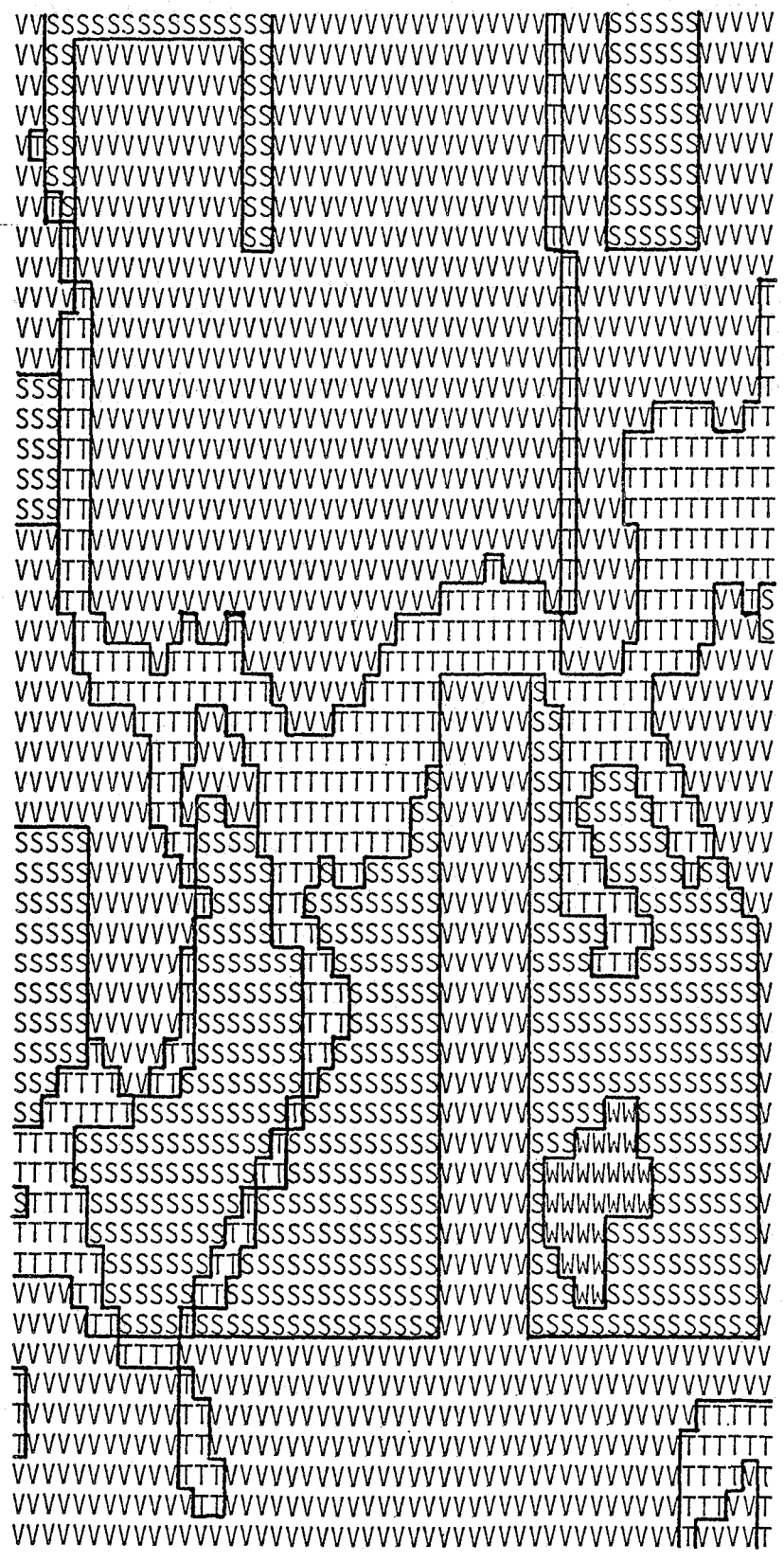

(a)

Fig. 14(a). Distribution of target categories across the floodplain data base.

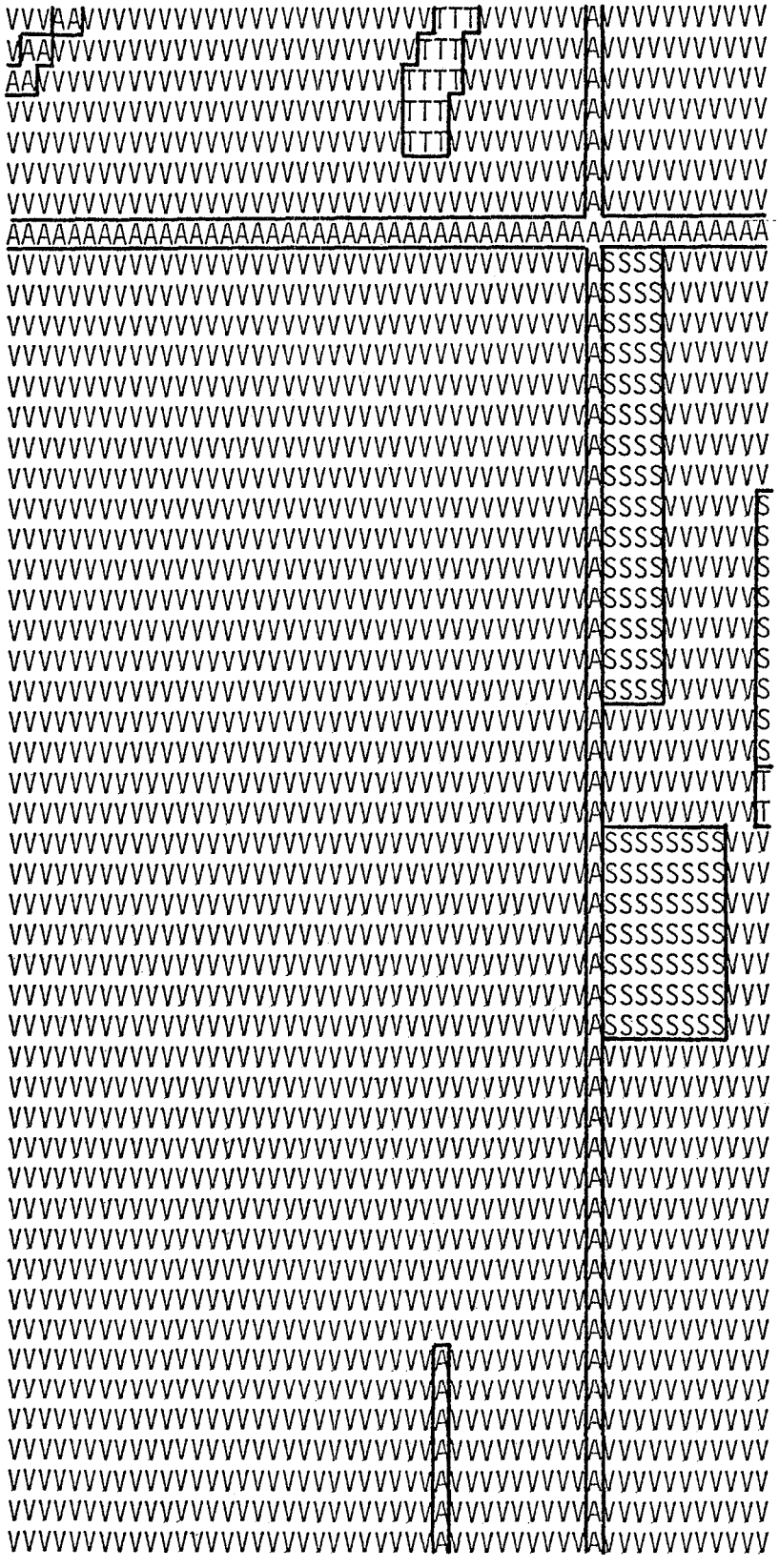

(b)

Fig. 14(b). Distribution of target categories across the hilly data base.

TABLE 3

Classification of Bare Soil According to Surface Roughness

Smooth	$0 < RMS \leq 2.0$ cm
Medium Rough	2.0 cm < RMS height $\leq$ 4.0 cm
Rough	4.0 cm < RMS height

TABLE 4

Classification of Vegetation-Covered Soil According to the Type of Vegetation

Mown Pasture
Pasture
Alfalfa
Wheat
Soybeans (N/S and E/W Rows)
Milo (N/S and E/W Rows)
Corn (N/S and E/W Rows)

TABLE 5

Statistics for Target Categories

Floodplain Data Base	Percentage
Rough Bare Soil	2.11
Medium-Rough Bare Soil	13.80
Smooth Bare Soil	9.30
Pasture	8.42
Soybeans N/S	1.00
Milo N/S	1.85
Corn E/W	11.23
Corn N/S	23.95
Wheat	10.69
Trees	16.53
River	1.12

Hilly Data Base	Percentage
Rough Bare Soil	0.62
Medium-Rough Bare Soil	2.54
Smooth Bare Soil	1.92
Pasture	5.38
Alfalfa	19.80
Soybeans E/W	3.04
Soybeans N/S	18.34
Milo E/W	3.96
Milo N/S	19.11
Wheat	15.38
Corn E/W	3.08
Corn N/S	1.61
Trees	0.85
Highway	4.38

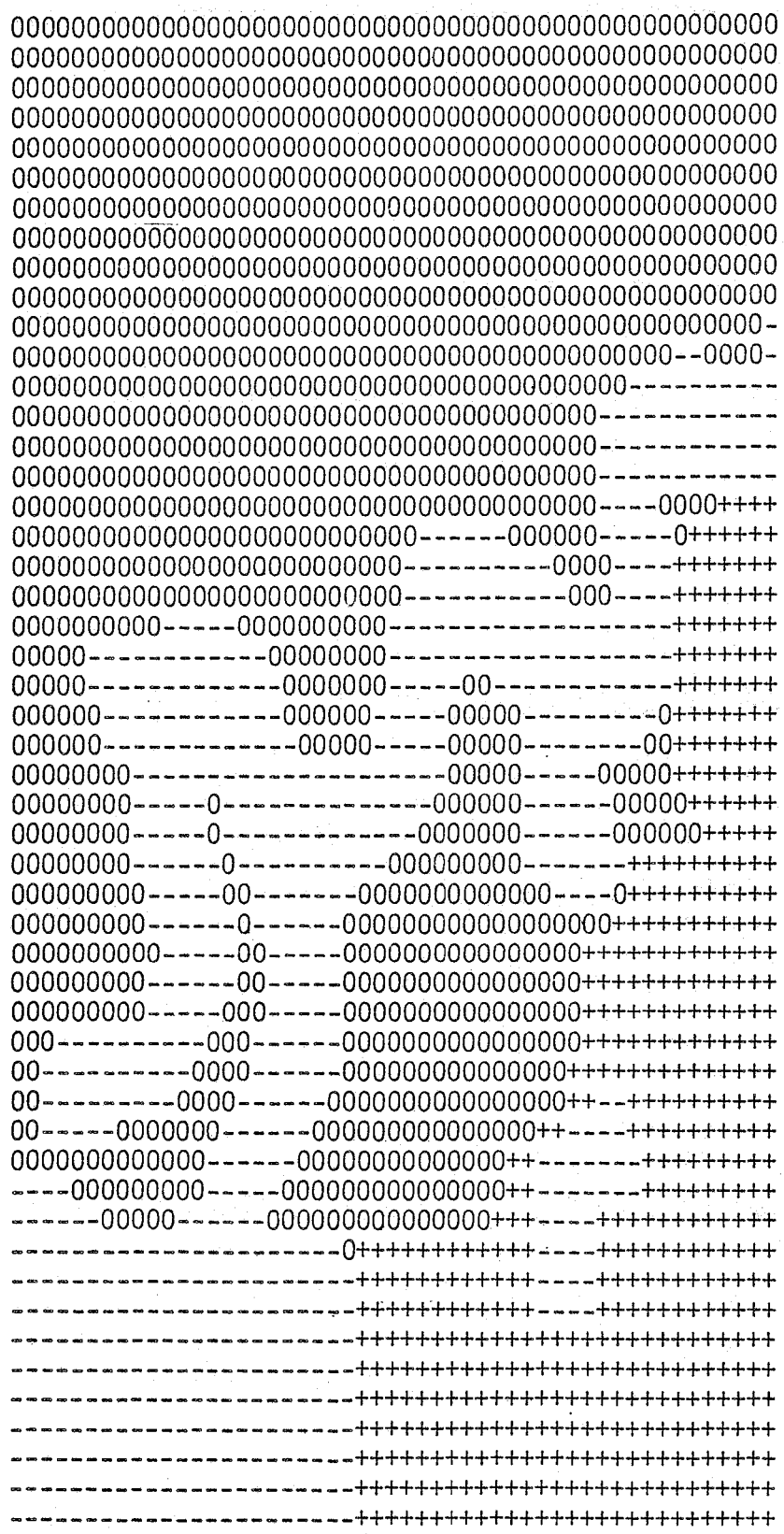

(a)

Fig. 15(a). Elevation distribution across the floodplain data base.

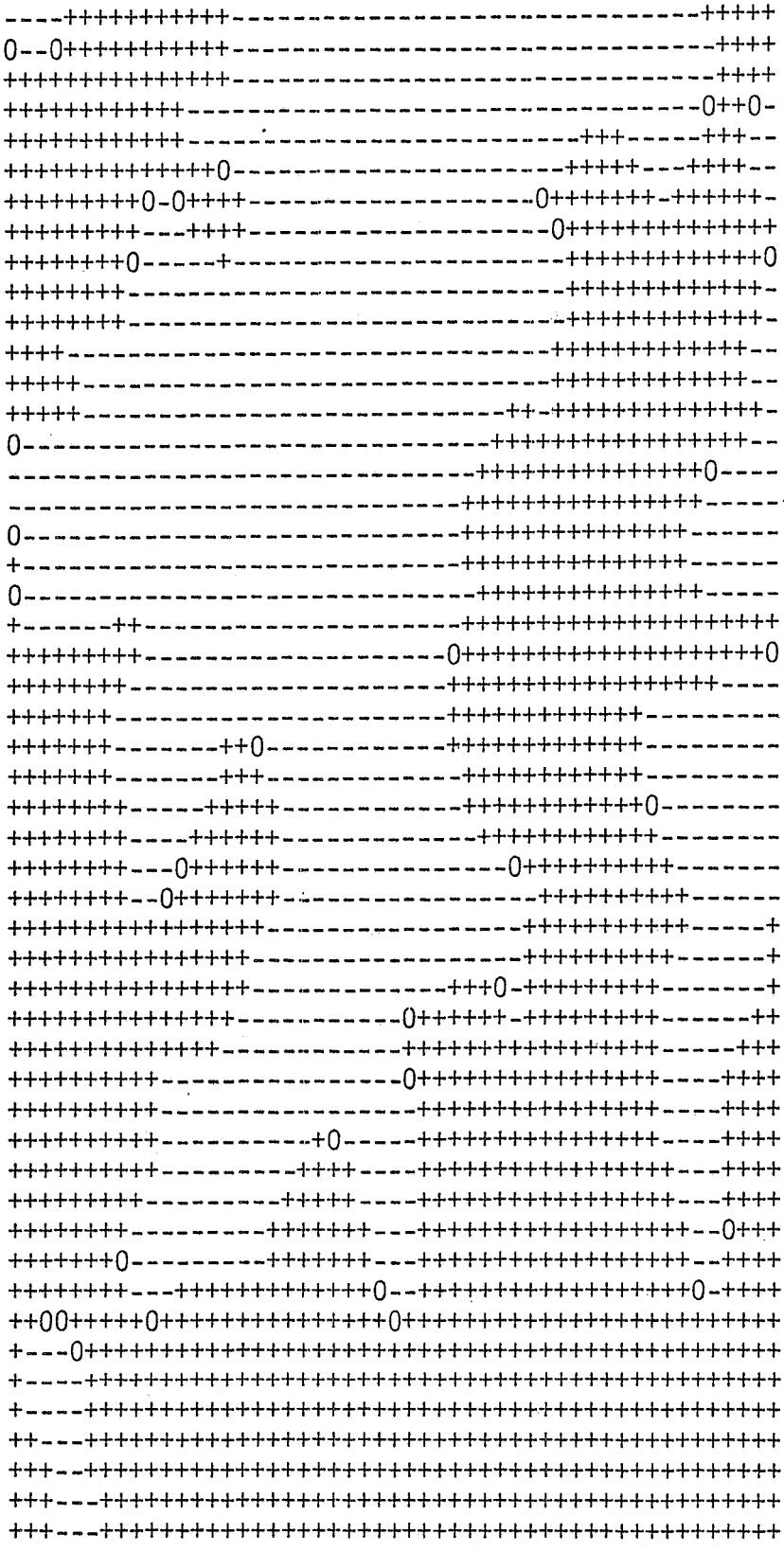

(b)

Fig. 15 (b). Elevation distribution across the hilly data base.

for the hilly area at each data-base cell. A zero (0) signifies that the elevation is simply the reference value described above. It can be seen clearly that the flat plain dominates the floodplain data base, especially in the northern half. The mean value and the standard deviation of elevation variations are 247.4 meters (811.8 feet) and 3.6 meters (11.95 feet) for the floodplain data base. For the hilly data base, they are 265.3 meters (870.5 feet) and 4.8 meters (15.74 feet), respectively, which indicates that the elevation variation is a little larger than it is for the floodplain data base.

In Fig. 16, distributions are shown for the elevation slope with respect to the surface distance in the across-track direction for both data bases; where a "+" means that the surface slope is toward the radar and a "-" means it is away from the radar. Zero indicates that there is no slope. By comparing the figures of the two data bases, one can again see the difference in the surface-elevation variations.

4.3 Backscattering Coefficients

The backscattering coefficient σ^o is the most significant value for the radar measurement of soil moisture. It varies with the contents of water along with the local angle of incidence, which is usually expressed by the following empirical form:

$$\sigma^o = f(\theta_\ell) + g(\theta_\ell) \times M_{FC} \qquad (11)$$

where σ^o is expressed in dB, $f(\theta_\ell)$ is the scattering coefficient at zero soil moisture as a function of local angle of incidence, $g(\theta_\ell)$ is the sensitivity of the scattering coefficient to soil moisture as a function of local angle of incidence, M_{FC} is the 0-5 cm soil moisture expressed

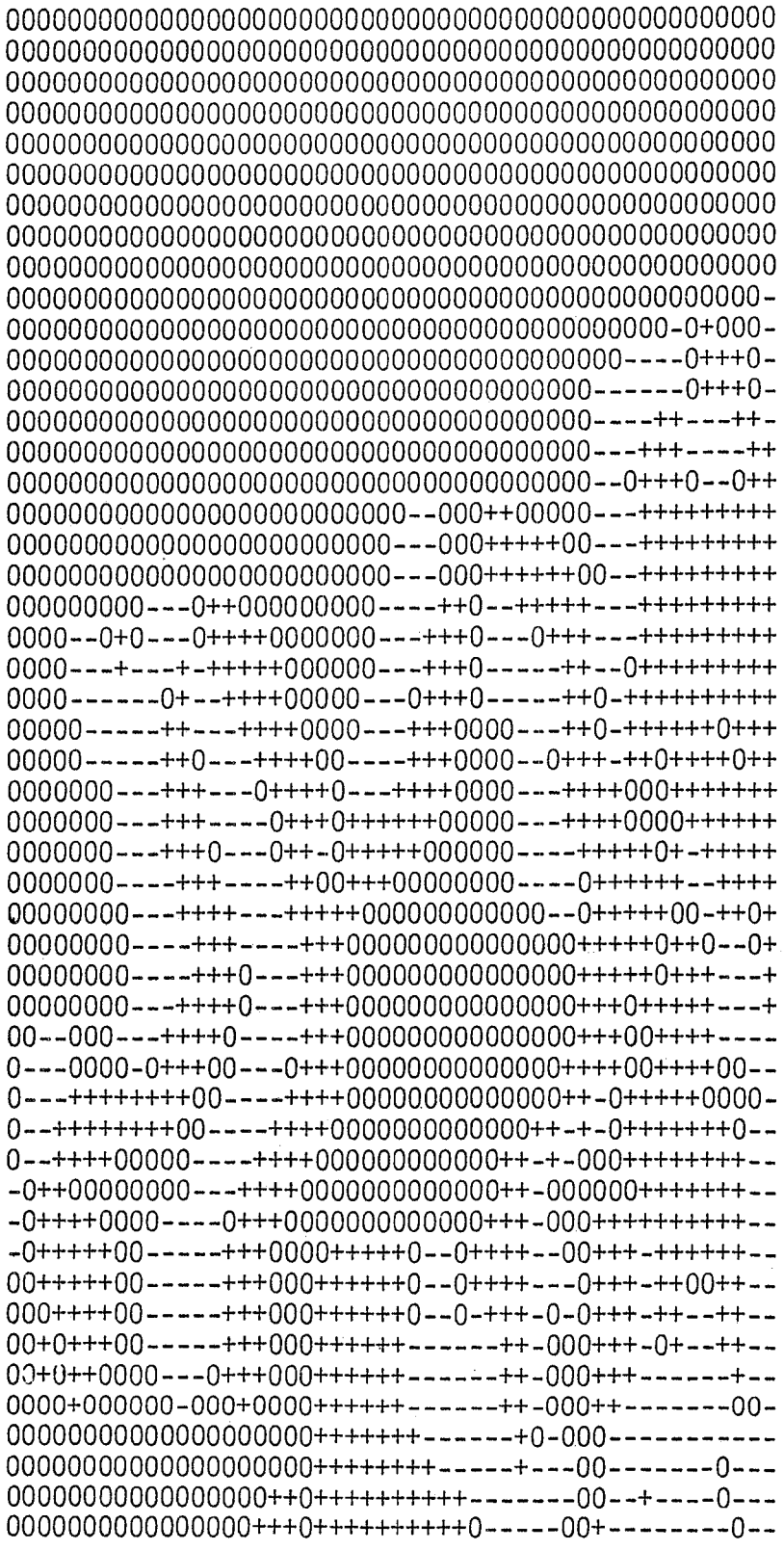

(a)

Fig. 16(a). Distribution of the elevation derivative in the across-track direction for the floodplain data base.

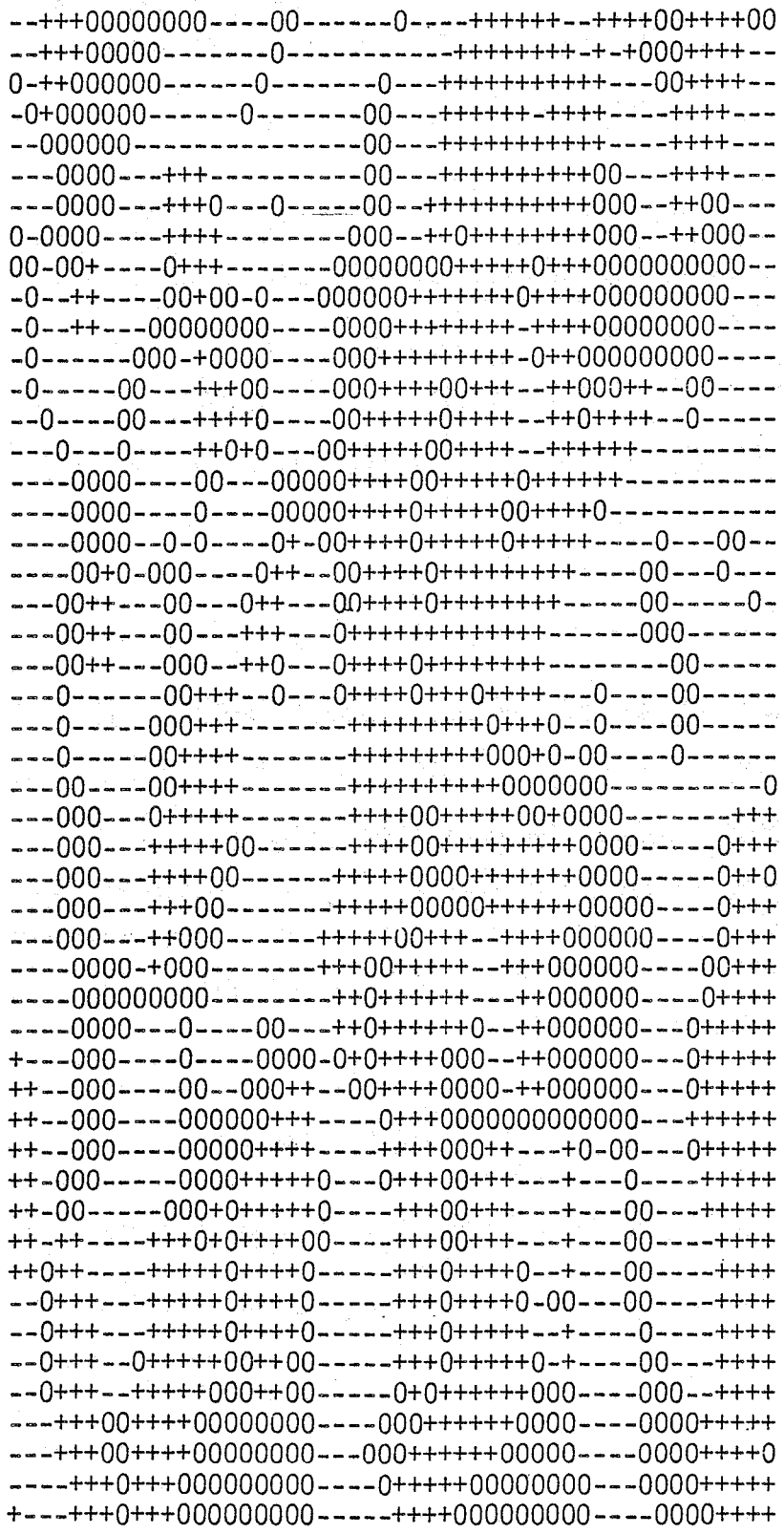

(b)

Fig. 16(b). Distribution of the elevation derivative in the across-track direction for the hilly data base.

as a percentage of the 1/3-bar water content and θ_ℓ is the local angle of incidence. Based on the large amount of experimental data relating the backscattering coefficients and the soil moisture at specific angles of incidence, $f(\theta_\ell)$ and $g(\theta_\ell)$ were determined empirically. The data collections were made at the frequencies between 4.25 GHz and 4.9 GHz with horizontal polarizations both for transmission and reception for each target category for which soil moisture could be defined. The measured data at the angles of incidence of 0, 10, 20, and 30 degrees as a function of M_{FC} are first submitted to a linear least-squares regression to establish the relationship between σ^o and M_{FC} at each angle of incidence. The linear regression coefficients of the above four angles are then fitted with third-order polynomials as a function of the angle of incidence to produce $f(\theta)$ and $g(\theta)$. Their forms are given as follows:

$$f(\theta) = f_1 + f_2\,\theta + f_3\,\theta^2 + f_4\,\theta^3 \tag{12}$$

$$g(\theta) = g_1 + g_2\,\theta + g_3\,\theta^2 + g_4\,\theta^3, \tag{13}$$

and the coefficients f_i ($i = 1, .., 4$) and g_i ($i = 1, .., 4$) for each target category are summarized in Table 6. For farmland having conspicuous row structure (soybeans, milo, and corn), determination of $f(\theta)$ is made separately, for both parallel and perpendicular radar look direction with respect to row structure. The $f(\theta)$ and $g(\theta)$ given here are valid only within the angular range of 0° to 30°.

The target categories where no water content is defined are trees, water bodies, and artificial objects. Among them, trees and water bodies have backscattering coefficients that vary with angle of incidence. For these targets, the backscattering coefficients are expressed by $f(\theta)$,

TABLE 6

Coefficients of the Algorithm for Computing the Backscattering Coefficient of Bare Soil and Vegetation-Covered Soil

Target Class	Roughness Class or Row Direction	Algorithm Coefficients*							
		$f(\theta)$				$g(\theta)$			
		f_1	f_2	$f_3 \times 10^{-2}$	$f_4 \times 10^{-3}$	g_1	$g_2 \times 10^{-2}$	$g_3 \times 10^{-3}$	$g_4 \times 10^{-5}$
Bare Soil	Smooth	- 5.13	- 1.961	8.59	- 1.375	0.182	- 0.122	- 0.123	0.287
	Medium Rough	-11.69	- 0.512	1.52	- 0.202	0.137	0.463	- 0.381	0.70
	Rough	-15.09	0.219	- 2.25	0.332	0.157	- 0.353	0.191	- 0.22
Mown Pasture	NA	- 5.13	- 1.961	8.59	- 1.375	0.182	- 0.122	- 0.123	0.287
Pasture	NA	- 1.675	- 3.045	19.8	- 3.674	0.107	2.522	- 2.523	5.278
Alfalfa	NA	- 1.675	- 3.045	19.8	- 3.674	0.107	2.522	- 2.523	5.278
Soybeans	Parallel	-10.00	- 0.591	2.81	- 0.509	0.181	- 0.614	0.041	0.228
	+Perpendicular	-10.00	- 0.574	3.31	- 0.676	0.181	- 0.614	0.041	0.228
Milo	Parallel	- 9.74	- 0.311	0.835	- 0.108	0.124	- 0.502	0.132	- 0.113
	+Perpendicular	- 9.74	- 0.294	1.34	- 0.275	0.124	- 0.502	0.132	- 0.113
Corn	Parallel	- 7.77	- 0.369	- 0.036	0.133	0.128	- 0.093	- 0.205	0.607
	+Perpendicular	- 7.77	- 0.352	0.464	- 0.034	0.128	- 0.093	- 0.205	0.607
Wheat		- 1.675	- 3.045	19.8	- 3.674	1.107	2.522	- 2.523	5.218
Sandbars		- 5.13	- 1.961	8.59	- 1.375	0.182	- 0.122	- 0.123	0.287

*See Eqs. 12 and 13

and are summarized in Table 7; the sensitivity terms against the water content $g(\theta)$ are put at zero. For artificial objects, such as roads, bridges, and buildings, the backscattering coefficients are assumed to be independent of the angle of incidence, and to be 10 dB as shown also in Table 7.

Figure 17 shows the backscattering coefficients of each target category as a function of the angle of incidence at soil moisture M_{FC} of 25% and 100%, and those values will be used for the simulations to follow.

The descriptions here are from Ulaby et al. (1981).

4.4 Determination of Local Angle of Incidence, Mean Elevation, and Effective Area

For purposes of computing the backscattered power by means of the radar equation shown below,

$$P_r = \frac{C\ A\ \sigma^o}{R^4} \tag{14}$$

the local angle of incidence, which is necessary to determine the backscattering coefficient; the mean elevation, which is necessary to calculate the distance R; and the effective area A must be determined. The data base provides information on the surface elevation at the lattice points of a mesh having 36-meter intervals in the along- and across-track directions as shown in Fig. 18.

The mean elevation of the (i,j)th cell is determined by averaging the elevations of the (i,j)th, (i+1,j)th, (i,j+1)th and (i+1,j+1)th lattice points as,

$$\overline{EL(i,j)} = \frac{EL(i,j) + EL(i+1,j) + EL(i,j+1) + EL(i+1,j+1)}{4} \tag{15}$$

TABLE 7

Algorithm for Computing the Backscattering Coefficient of the Target, Where no Water Content Can be Defined

Target Class	$f(\theta)$*
Water Bodies	$22.82 - 5.126\theta + 0.237\theta^2 - 3.973 \times 10^{-3}\theta^3$
Deciduous Trees	$10 \log (10^{-1.143} \times \cos\theta)$

Target Class	Constant Value (dB)
Railroads	10.0
Bridges	10.0
Buildings	10.0
Highways	10.0

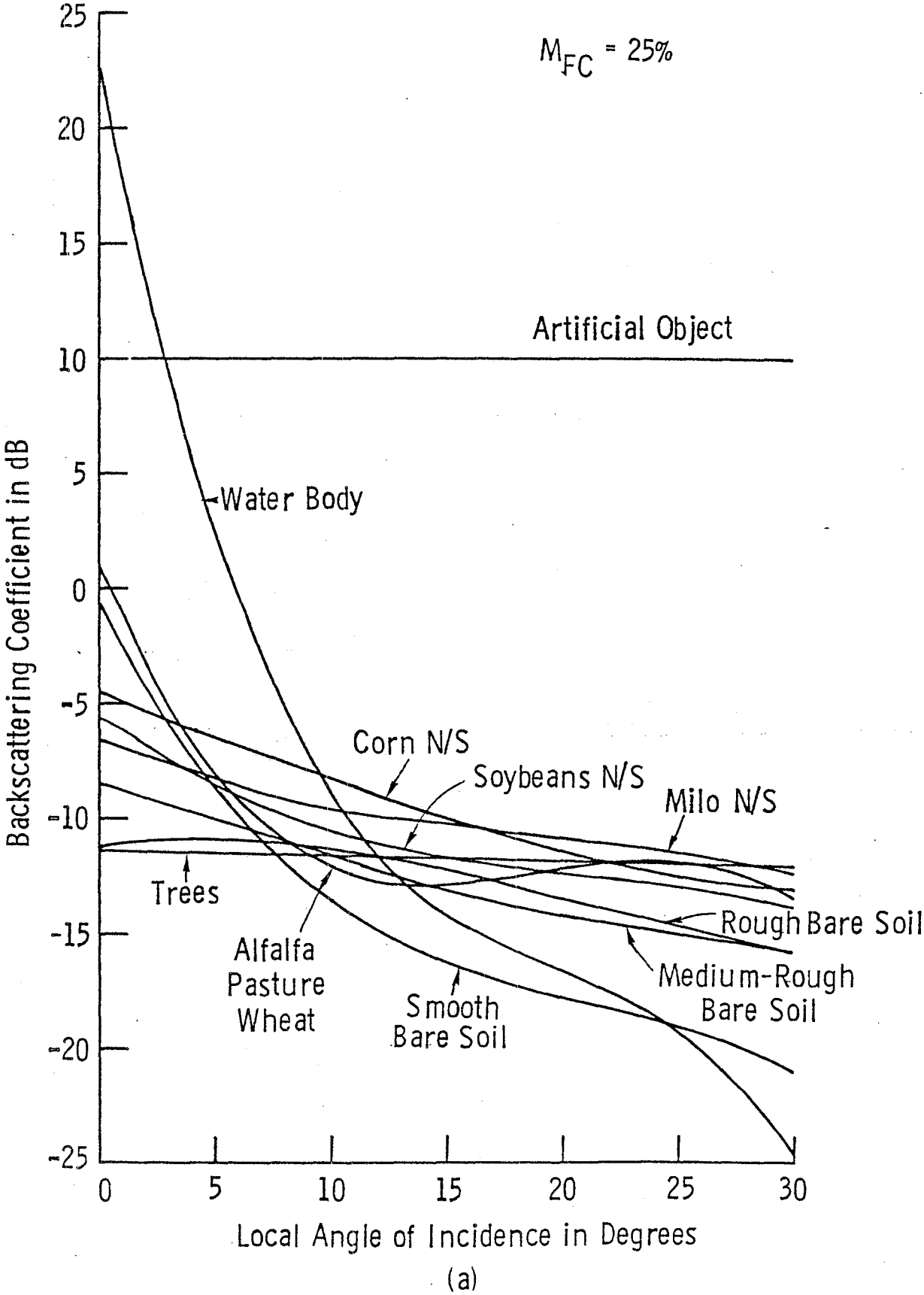

(a)

Fig. 17(a). Backscattering coefficients of some target categories at M_{FC} = 25% as a function of the local angle of incidence.

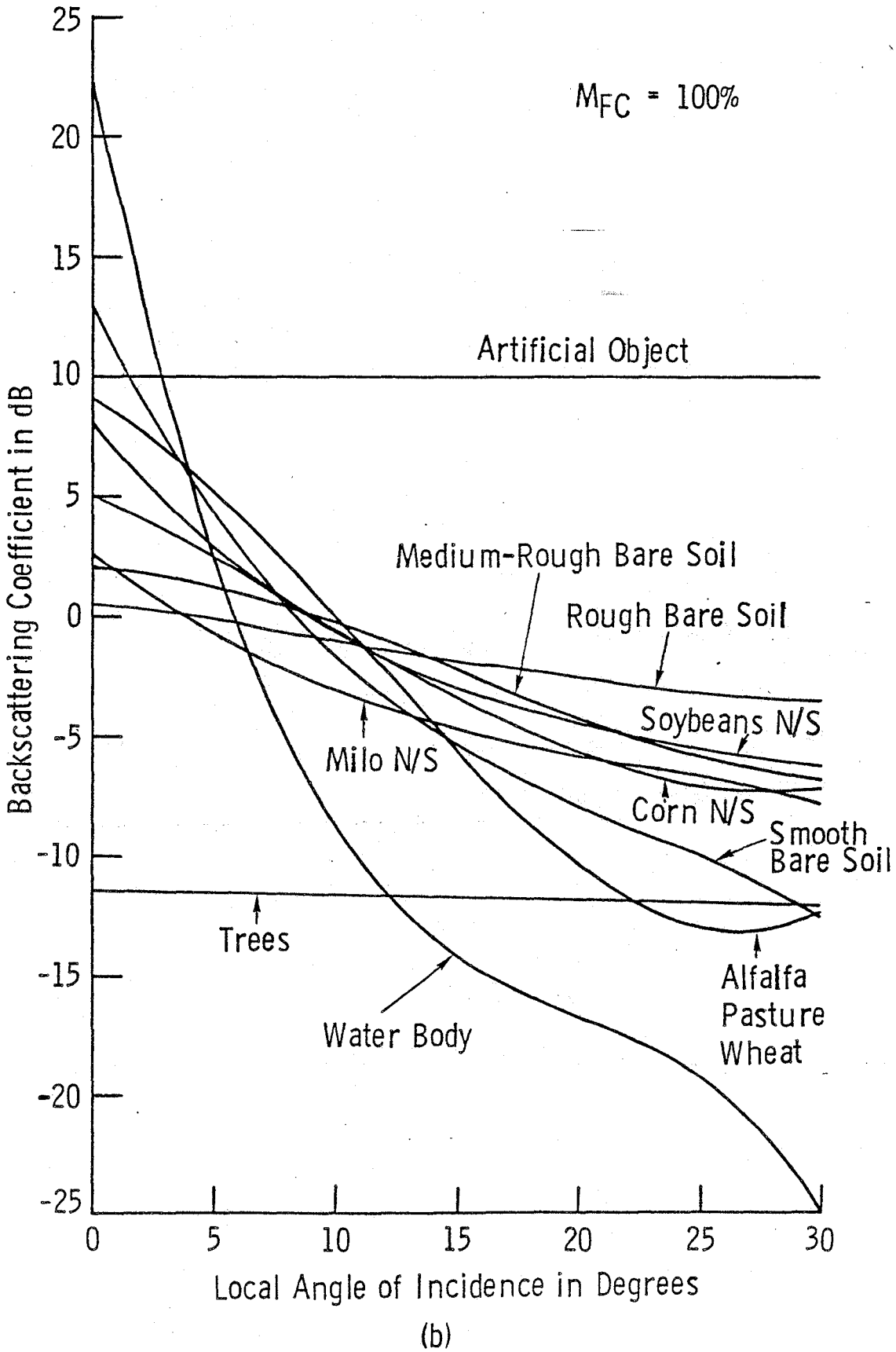

(b)

Fig. 17(b). Backscattering coefficients of some target categories at M_{FC} = 100% as a function of the local angle of incidence.

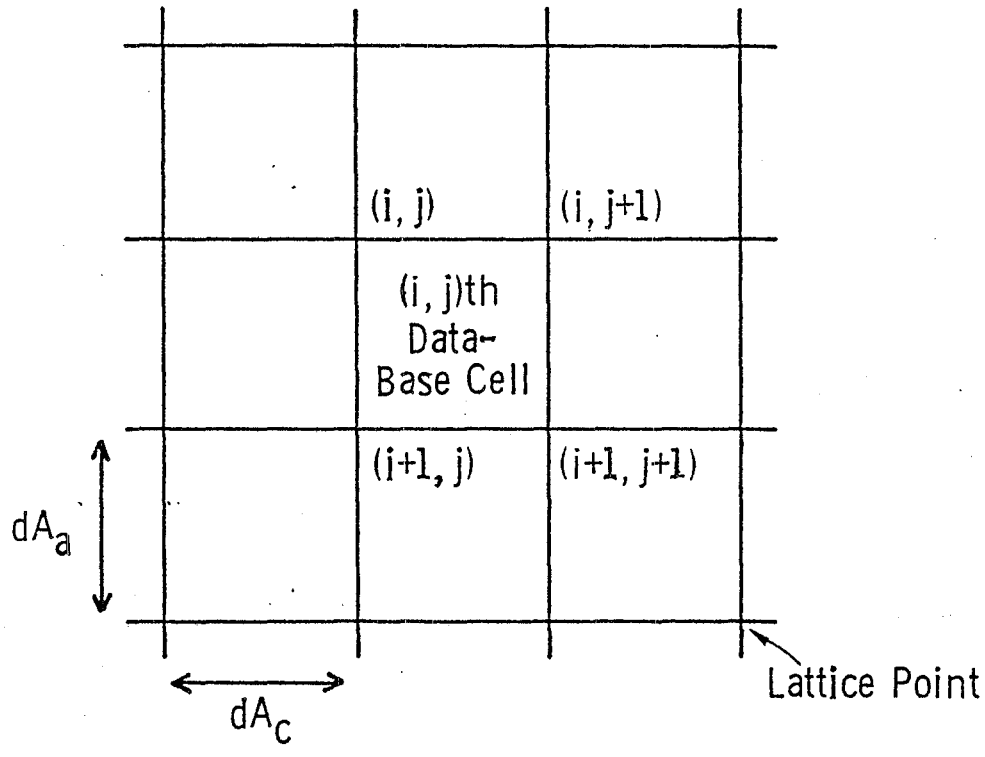

Fig. 18. Data-base lattice points and cells. Surface elevations are specified at each lattice point.

at the very center of the four lattice points. By using this mean elevation, we can calculate the distance between the radar and the target area, and then specify the appropriate range bin for SAR processing.

The local slopes in the along- and across-track directions are calculated by a linear approximation as follows:

$$\tan\alpha = \frac{\frac{EL(i+1,j) + EL(i+1,j+1)}{2} - \frac{EL(i,j) + EL(i,j+1)}{2}}{dA_a} \qquad (16)$$

$$\tan\beta = \frac{\frac{EL(i,j+1) + EL(i+1,j+1)}{2} - \frac{EL(i,j) + EL(i+1,j)}{2}}{dA_c} \qquad (17)$$

where α and β are the inclination angles of the surface, and dA_a and dA_c are the length of the data-base cell in the along- and across-track directions, respectively. The local angle of incidence of the surface can be derived as a function of α and β as follows (Holtzman et al., 1977; Ulaby et al., 1981):

$$\theta_\ell = \cos^{-1} \frac{\tan\beta \sin\theta + \cos\theta}{\sqrt{\tan^2\alpha + \tan^2\beta + 1}} \qquad (18)$$

where θ_ℓ is the local angle of incidence and θ the angle of incidence when no surface slopes exist. By introducing this local angle of incidence into the algorithms of the backscattering coefficient, we can obtain the mean value of the backscattering coefficient at the data-base cell.

The effective area A can also be determined by the following equation:

$$A = \frac{dA_a}{\cos\alpha} \times \frac{dA_c}{\cos\beta} . \qquad (19)$$

In the present simulations, the data-base cell is assumed to be 36-m x 36-m, so that dA_a and dA_c are 36 meters for Eqs. 16, 17, and 19.

The (i,j)th data of the target category are assigned to the data-base cell surrounded by the four lattice points of the (i,j)th, (i+1,j)th, (i,j+1)th and (i+1,j+1)th cells. By using these quantities, we can calculate the backscattered power at each data-base cell.

4.5 Simulation of Fading

In radar measurements, fading of the received signal is inherent, especially for a SAR. Therefore, the effect of fading must be included in the radar simulation package to simulate exactly the behavior and the performance of the SAR with respect to an actual target. This effect is not included in the previously described simulation package, since it was used for developing the package itself. The fading that appeared in the radar measurements is shown to obey the Rayleigh distribution in power, and we can simulate it by using two Gaussian distributions for in-phase and quadrature components (Ulaby et al., 1981).

The mean received power $\overline{P_r}$ is written in terms of the in-phase and quadrature components, V_I and V_Q, as follows:

$$P_r = V_I^2 + V_Q^2. \tag{20}$$

To accommodate the effect of fading, the mean received power is again divided into two orthogonal components as,

$$E_I = \sqrt{\frac{\overline{P_r}}{2}}\ \mu_1(0,1) \tag{21}$$

$$E_Q = \sqrt{\frac{\overline{P_r}}{2}}\ \mu_2(0,1), \tag{22}$$

where $\mu_i(0,1)$, $i = 1, 2$ signifies the Gaussian random numbers of zero mean, having a standard deviation of one. From Eqs. 21 and 22, the simulated received power is expressed by the following equation:

$$P_r = E_I^2 + E_Q^2 = \frac{\overline{P_r}}{2} (\mu_1^2(0,1) + \mu_2^2(0,1)). \tag{23}$$

The Gaussian random numbers are computer-generated.

4.6 Multilook Processor

Fading causes so-called "speckle" in a SAR image. Bright and dark spots in the image make it hard to distinguish the targets of the image; therefore, this can result in an error in the estimation of the level of soil moisture in the present problem. The technique of noncoherent averaging is used to reduce the effect of fading by averaging the received powers of some of the resolution cells. The effect of fading can be further reduced by increasing the number of cells to be averaged; however, the resolution then becomes poor. In the present simulations, the basic (one-look) resolution cell is 36 m x 36 m in size for the 1.8-km x 1.8-km data base, having 2500 cells. If a large number of cells is submitted to averaging, the number of cells after averaging becomes small, which may reduce the statistical significance of the following analysis. The four-look processor is, therefore, developed as a compromise between reducing the fading effects and keeping statistical significance.

Two of the four looks are picked up from the along-track direction and the rest are from the across-track direction, as shown in Fig. 19. The final resolution cell, therefore, becomes 72 m x 72 m, which provides 625 cells across the entire data base.

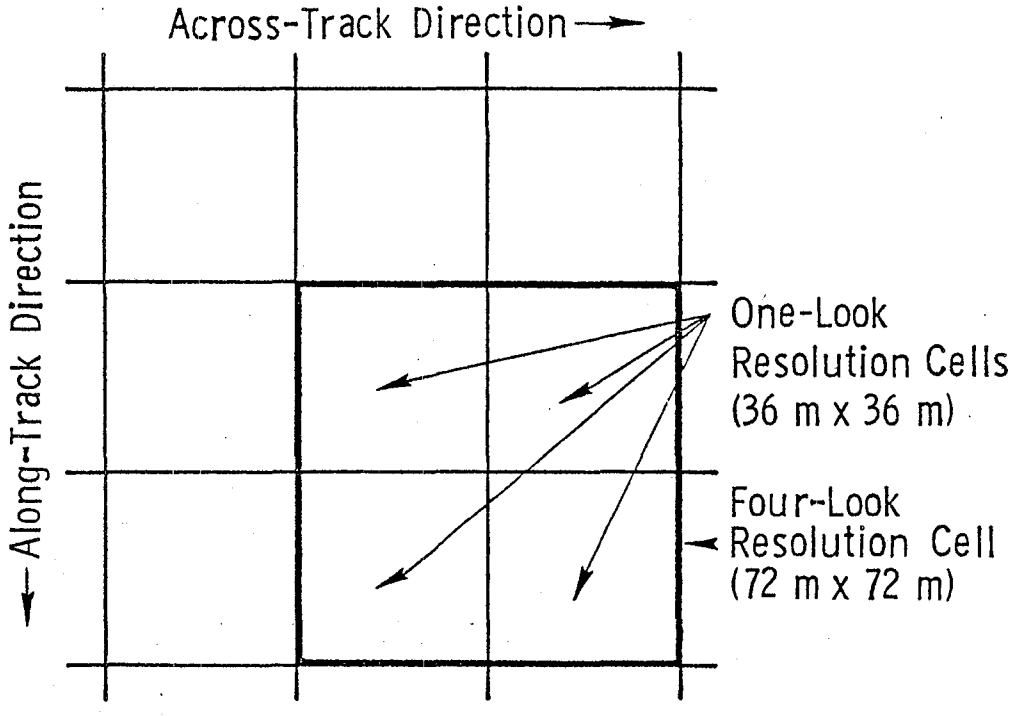

Fig. 19. Averaging of four one-look resolution cells to make a four-look resolution cell.

4.7 Estimation Algorithm for Soil Moisture

In a SAR, the scattering coefficient, σ^o, can be calculated for each resolution cell by solving the radar equation. The radar equation is again written simply as follows:

$$P_r = \frac{C\ A\ \sigma^o}{R^4} \quad . \tag{14}$$

For convenience, in the simulations C is chosen to be equal to R_o^4 where R_o is the distance between the radar trajectory and the center of the assumed data base.

For remote-sensing situations, the surface elevation is usually unknown at the processor, so the effective area A is chosen as the theoretical value for a surface without elevation variations. In addition, because the difference between R^4 for the farthest and R^4 for the nearest resolution cell is very small compared with R_o^4 (about 0.16%), $R = R_o$ is used for all cells.

The scattering coefficient σ^o is then calculated as follows:

$$\sigma^o = \frac{P_r}{A} \quad . \tag{24}$$

The soil-moisture estimation algorithms are applied to the above-calculated scattering coefficient σ^o to estimate the soil moisture in the form of percent M_{FC}. The algorithms are for bare soil, vegetation-covered soil, and the two together. For developing the algorithms, the experimental data at the angles of incidence of 0°, 10°, 20°, and 30° are submitted to least-squares linear regression to establish the linear dependence of σ^o on percent M_{FC}. The results are then introduced into the third-order polynomial fitting to determine the relationship between

σ^o and the percent M_{FC} as a function of the angle of incidence. The general form used to relate σ^o to percent M_{FC} is the same as that described previously,

$$\sigma^o = f(\theta) + g(\theta) \times M_{FC} \ . \tag{11}$$

Rearranging the terms of the above equation, we can obtain the general form of the soil moisture estimation algorithm as follows:

$$M_{FC} = \frac{(\sigma^o - f(\theta))}{g(\theta)} \ . \tag{25}$$

The $f(\theta)$ and $g(\theta)$ functions have the form of Eqs. 12 and 13. The coefficients of the algorithms for the general case, including bare soil and vegetation-covered soil, are listed in Table 8.

Figure 20 shows the estimated M_{FC} against σ^o at an angle of incidence of 7.5 degrees, which is the value chosen for the simulations. The sensitivity of the estimated M_{FC} with respect to σ^o is a little higher for the vegetation-covered soil than for the bare soil; however, the difference is not very significiant. The curve for the agricultural target, including both bare and vegetation-covered soil, lies between the curves for bare soil only and for vegetation-covered soil only.

4.8 Results and Discussion

The computer simulations are carried out against the two data bases in order to evaluate the ability of a SAR to detect soil moisture in the actual environment. The soil moistures, M_{FC}, in the data bases are assumed to be 25% and 100% to simulate dry- and wet-soil conditions, respectively. A detailed explanation of the simulation package can be found in the Appendix.

TABLE 8

Coefficients of the Algorithms for Estimating Soil Moisture

Agricultural Scene Classes	$f(\theta)$, intercept in dB	$g(\theta)$, slope in dB/1.0% M_{FC}
All agricultural scene data	$-9.666-8.432\times10^{-1}\theta+4.587\times10^{-2}\theta^2-8.272\times10^{-4}\theta^3$	$.1615+9.383\times10^{-4}\theta-4.975\times10^{-4}\theta^2+1.207\times10^{-5}\theta^3$
Bare soil data only	$-10.92-8.366\times10^{-1}\theta+4.0635\times10^{-2}\theta^2-7.838\times10^{-4}\theta^3$	$.1697+6.017\times10^{-4}\theta-3.755\times10^{-4}\theta^2+1.003\times10^{-5}\theta^3$
Crop canopy data only	$-9.377-9.572\times10^{-1}\theta+6.339\times10^{-2}\theta^2-1.233\times10^{-3}\theta^3$	$.1653+3.997\times10^{-3}\theta-9.47\times10^{-4}\theta^2+2.273\times10^{-5}\theta^3$

TABLE 9

Correspondence Between the Symbols in the Soil Moisture Estimation Map and the Ranges of Estimation Error Relative to the Assumed Soil Moisture

Symbol	Range of Estimation Error (E.E.)
-	E.E. < -100%
0	-100% ≤ E.E. < - 80%
1	- 80% ≤ E.E. < - 60%
2	- 60% ≤ E.E. < - 40%
3	- 40% ≤ E.E. < - 20%
4	- 20% ≤ E.E. < 0%
5	0% ≤ E.E. < 20%
6	20% ≤ E.E. < 40%
7	40% ≤ E.E. < 60%
8	60% ≤ E.E. < 80%
9	80% ≤ E.E. < 100%
+	100% ≤ E.E.

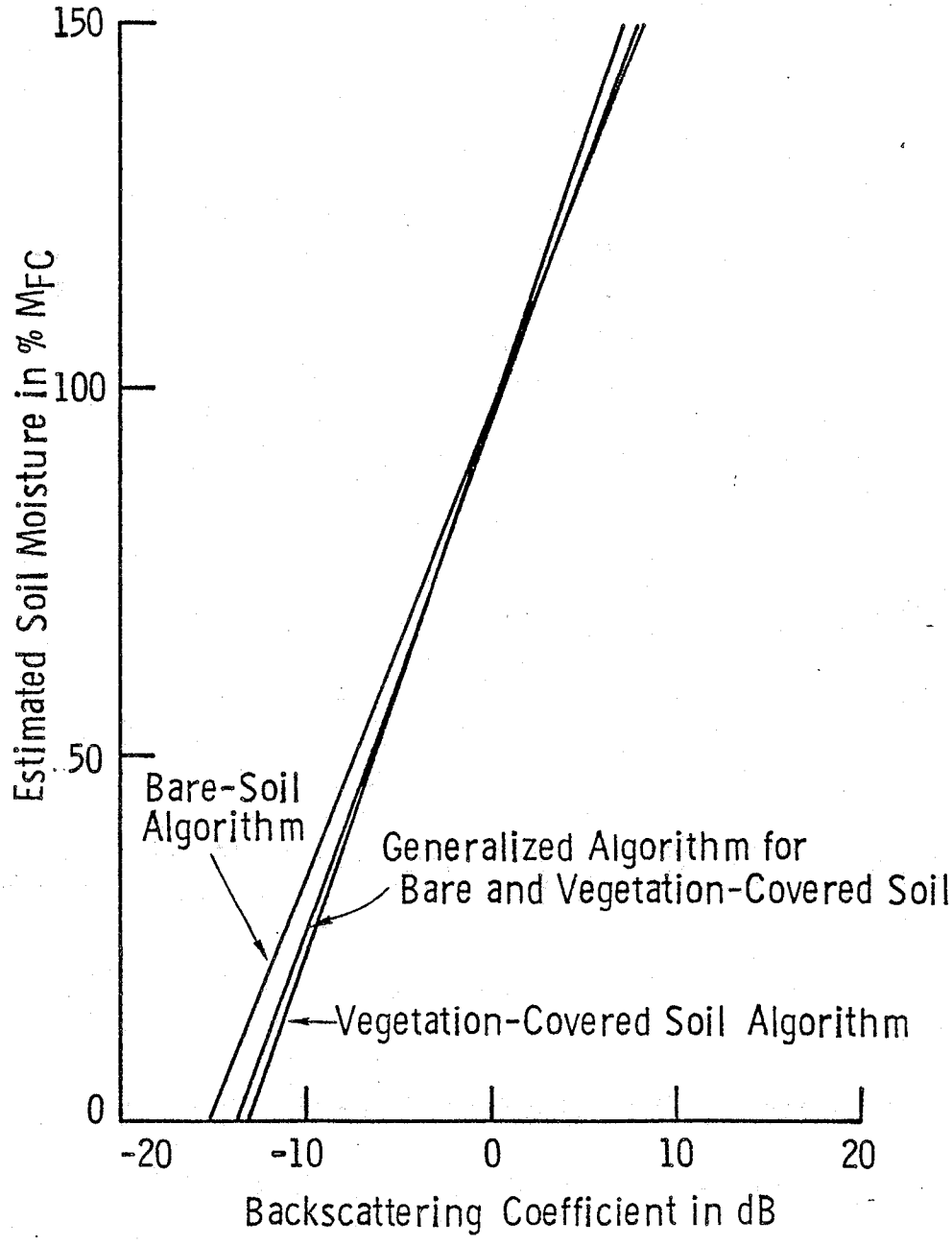

Fig. 20. Backscattering coefficient versus estimated soil moisture at a local angle of incidence of 7.5°.

Figure 21 shows the results of soil moisture estimation by means of computer simulation at M_{FC} = 25% and 100% for the floodplain data base. The estimations are made under the assumption that no *a priori* information about land usage is available. Each letter represents the 72-m x 72-m resolution cell and its value denotes the estimated soil moisture. In Table 9, a correspondence is shown between the letter and the range of the percentage of M_{FC} relative to the assumed value. The color yellow is assigned to the resolution cell where the estimation error of soil moisture is within ±20% of the estimated and assumed M_{FC} (4 and 5). In the red regions, M_{FC} is overestimated in excess of 20% (6, 7, 8, 9, +), and underestimated by more than 20% in the blue regions (-, 0, 1, 2, 3).

In the results for M_{FC} = 100%, the underestimated area having the numbers -, 0, 1, 2, and 3 (blue areas) corresponds well to the tree category referring to Fig. 14. The backscattering coefficient for trees is smaller than that for bare soil and vegetation-covered soil at an angle of incidence of 7.5 degrees (see Fig. 17), so that the backscattered powers at the cells are small, which results in an apparently low estimation of soil moisture. No such clear trend can be seen in the results for the M_{FC} = 25% map, since the scattering coefficient for trees is closer to that for bare soil and vegetation-covered soil at M_{FC} = 25%. The overestimated area located at the bottom center of the M_{FC} = 100% map may be due to the topographic effect where the slope runs toward the radar (see Fig. 16). At these sites, the local angle of incidence becomes small, i.e., closer to vertical, so the backscattered powers become higher than for the flat surface, which results in the overestimation of soil moisture.

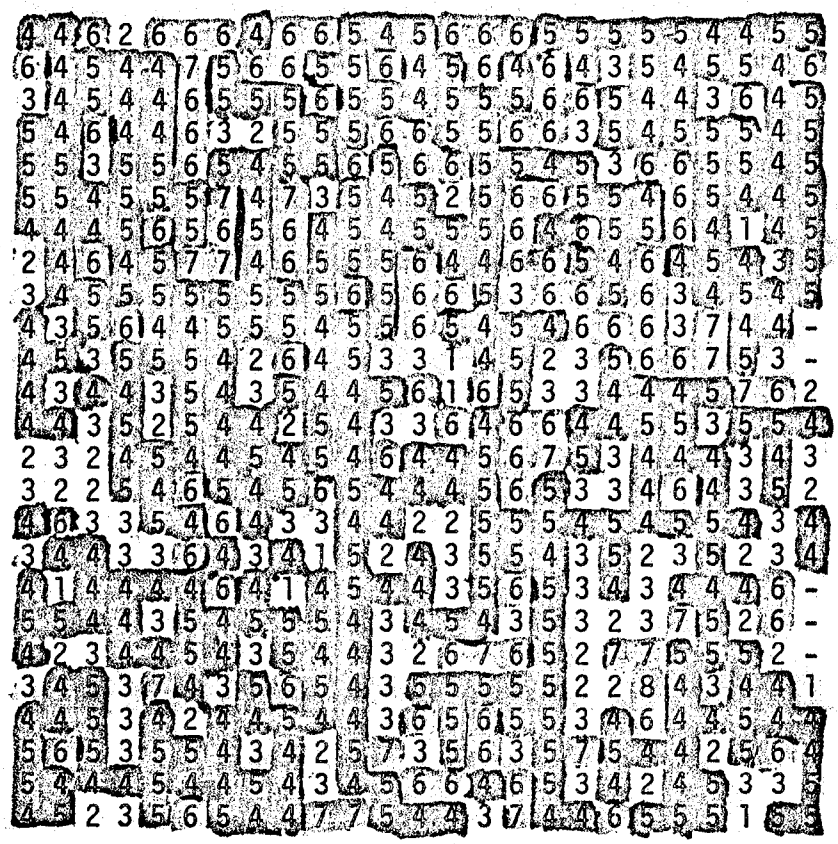

(a)

Fig. 21(a). Distribution of estimated soil moisture for the floodplain data base at M_{FC} = 25%.

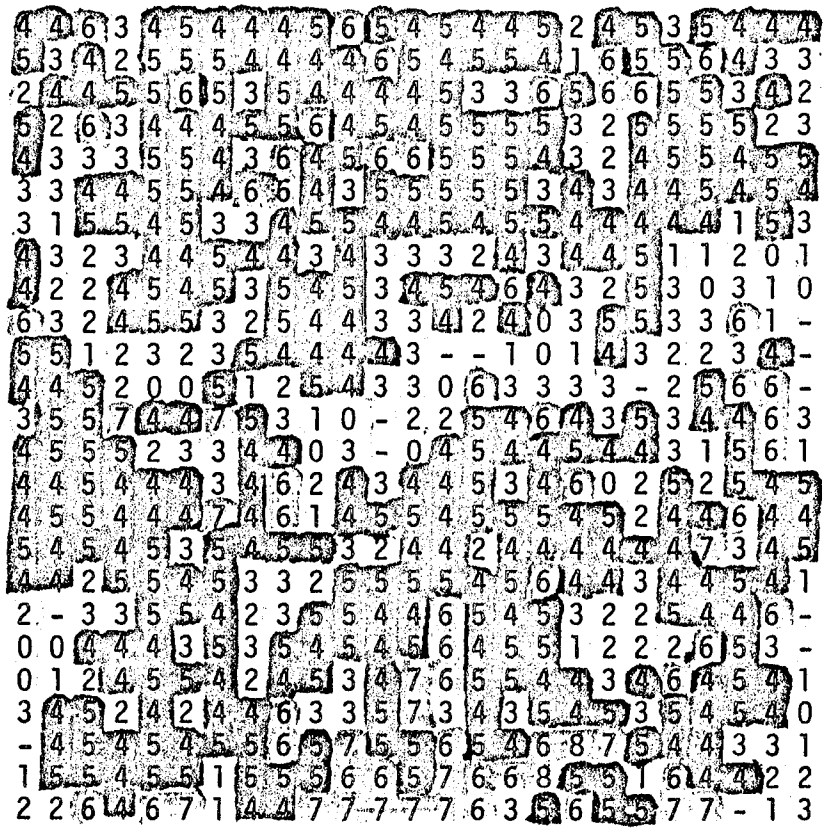

(b)

Fig. 21(b). Distribution of estimated soil moisture for the floodplain data base at M_{FC} = 100%.

However, the tendency to underestimate is not clearly seen in the backslope region. This may be due to the difference in the angles of the slopes. The water bodies can be recognized in the M_{FC} = 100% map because of their relatively small backscattering coefficient as compared with bare soil and vegetation-covered soil; however, they are hard to distinguish in the M_{FC} = 25% map because the value of the backscattering coefficient of the water body is nearly the same as those for bare soil and vegetation-covered soil (see Fig. 17).

The region with a soil moisture estimation error of within ±20% dominates the flat plain (upper half of Fig. 21), as expected, for the M_{FC} = 100% map; however, this tendency is not necessarily clear in the M_{FC} = 25% map. The overestimation area is in greater evidence in the M_{FC} = 100% map (in the upper half) than in the M_{FC} = 25% map, but is not as severe.

Figure 22 shows the simulation results for the hilly data base. It can be easily seen that the area having the yellow color (symbolized by the numbers 4 and 5) is narrower than for both cases in the floodplain data base. In the M_{FC} = 25% map, the red horizontal and vertical lines having a plus sign correspond to the artificial object (road) which has a higher backscattering coefficient than those of the surrounding objects. Therefore, it results in an apparent overestimation of soil moisture by the blind classifier, in spite of the fact that no water content can be defined. The overestimation areas in the center and the lower-left portions of the map seem almost to correspond to the area having slopes that run toward the radar. It may, therefore, be possible that these overestimations occur because the local angle of incidence is closer to vertical, so that the backscattering

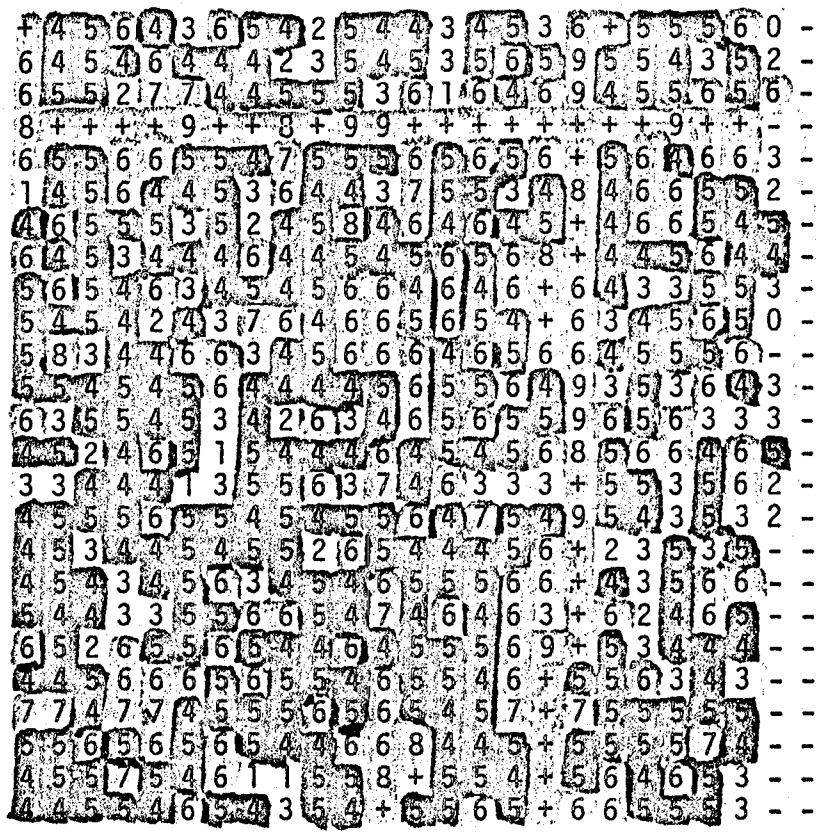

(a)

Fig. 22(a). Distribution of estimated soil moisture for the hilly data base at M_{FC} = 25%.

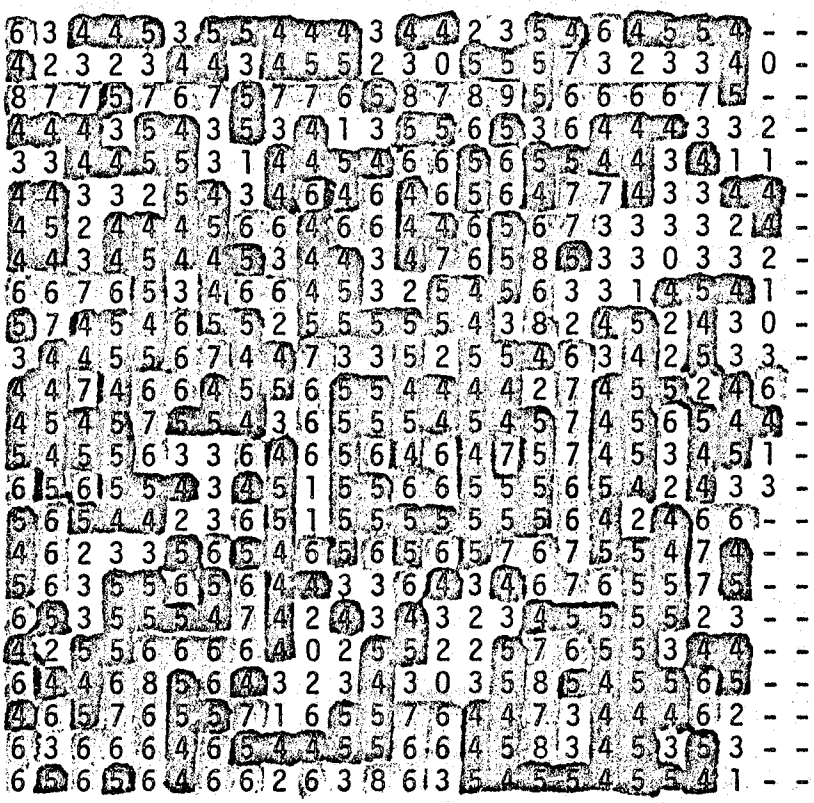

(b)

Fig. 22(b). Distribution of estimated soil moisture for the hilly data base at M_{FC} = 100%.

coefficient increases more than that for the 7.5-degree angle of incidence. However, there is no such clear trend for the backslope region. The road images do not appear clearly in the M_{FC} = 100% map as compared with the M_{FC} = 25% map, since the backscattering coefficients of bare soil and vegetation-covered soil approach that of a road when M_{FC} = 100%. This makes it a little difficult to distinguish the road from the other agricultural land. However, the road images can still be recognized when the image is compared with a land-use map (Fig. 14). The underestimation areas on the extreme right-hand sides of both maps in Fig. 22 are due to the lack of data at these locations as a result of the effect of range creep.

By comparing the maps in Figs. 21 and 22, the yellow areas (estimation error within ±20% in the difference between the estimated and assumed soil moisture) are wider for the floodplain data base than for the hilly data base, as expected. Figure 23 shows the cumulative distributions of the absolute value of the estimation error in M_{FC}, and percentages for specific values of estimation error are listed in Table 10. Using a small value for the estimation error (i.e., within ±20%), a more accurate estimation of soil moisture can be made for the floodplain data base than for the hilly data base, and for M_{FC} = 25% than for M_{FC} = 100%. The superiority of the floodplain data base over the hilly data base can be interpreted as being due to the difference in the elevation variation of the surfaces, which causes the range-creep effect; and that of M_{FC} = 25% over M_{FC} = 100% as being due to the reduced effect of the sidelobes, since the backscattering coefficients of the surroundings are smaller at M_{FC} = 25% than they are at M_{FC} = 100%.

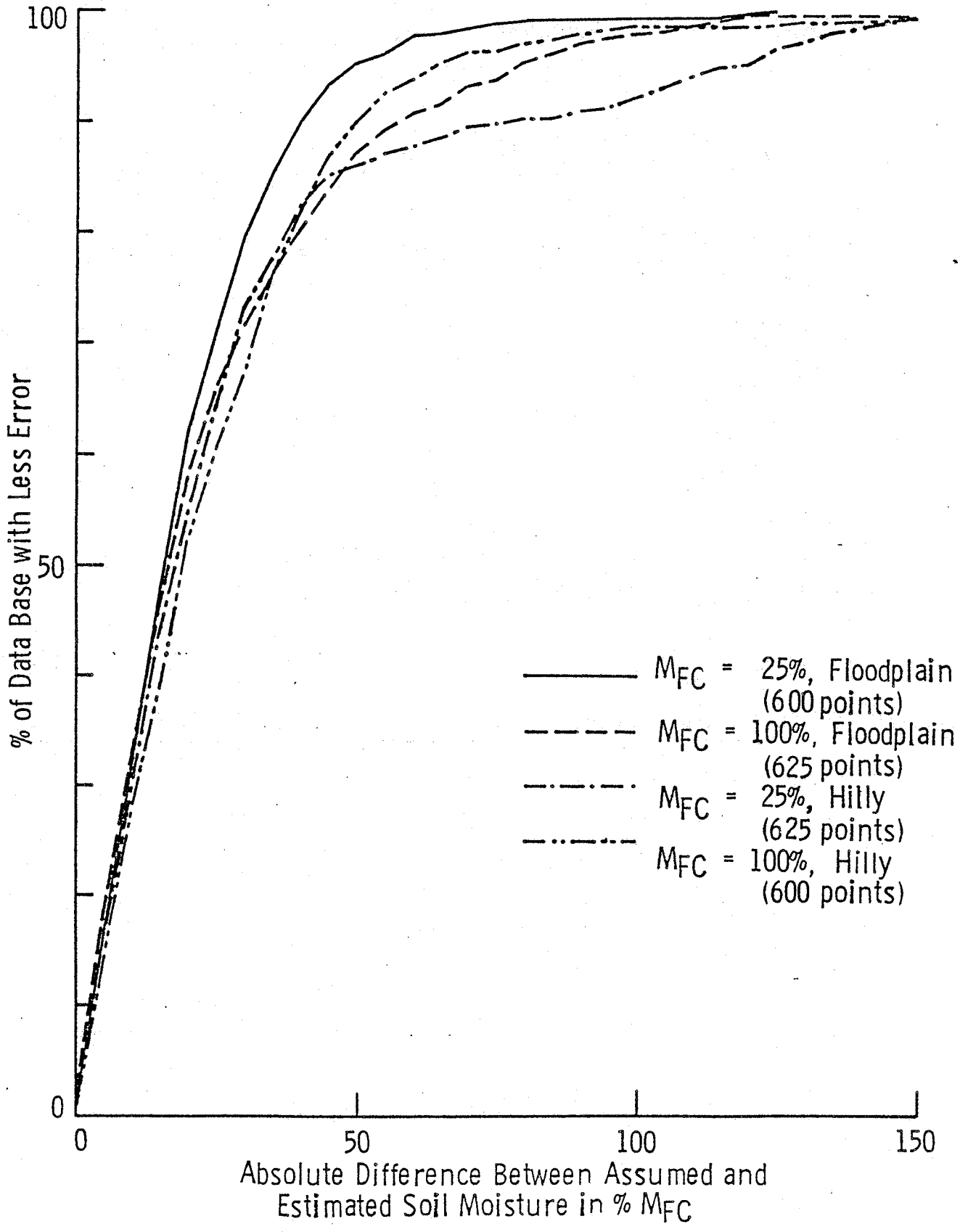

Fig. 23. Cumulative distributions of the absolute difference between assumed and estimated M_{FC}.

TABLE 10

Summary of the Estimation Error of Soil Moisture. Estimation is Made by Using a Generalized Algorithm and no *a priori* Knowledge about the Surface Usage is Available.

Absolute Value of Estimation Error	Floodplain		Hilly	
	Assumed M_{FC}		Assumed M_{FC}	
	25%	100%	25%	100%
0	1.9	2.1	1.2	1.3
5	17.1	18.7	17.3	15.5
10	31.5	33.4	30.8	28.3
15	47.7	46.1	44.0	39.5
20	62.1	58.2	54.8	52.3
25	70.9	66.1	64.5	61.0
30	79.4	71.7	73.5	67.7
35	85.3	76.2	77.8	76.5
40	89.9	80.2	82.7	82.3
45	93.4	84.0	85.3	87.0
50	95.4	87.2	86.2	90.2
55	96.3	89.4	87.2	92.5
60	97.8	90.9	87.8	93.8

In the M_{FC} = 25% map for the hilly data base, the effect of artificial objects and elevation variation may degrade the ability of the SAR to estimate soil moisture. In the M_{FC} = 100% map, however, the back-scattering coefficients for bare soil and vegetation-covered soil are close to those for artificial objects, so the estimation error appears to be smaller.

Figure 24 shows the cumulative distributions of estimation error in soil moisture when the distribution of land usage across the data bases is known *a priori*. This knowledge pertains, however, only to their distribution as projects onto a flat earth, so that if the target locations on the images move from their original locations due to the effect of foreshortening, we cannot discard the target cells in which no water can be statistically defined. In addition, the effect of the slopes may degrade the performance of the SAR for use in soil moisture estimation, especially for the hilly data base. This trend can be seen clearly in Fig. 24 and Table 11, where some percentages are listed at certain values for estimation errors.

The amount of data included in the above statistics is sufficiently small (when compared with the previous results [Ulaby et al., 1981]), that it is a little risky to make a direct comparison. In addition, a difference in the category of distribution across the data base exists, so that a comparison is made between only one of the present results (the floodplain data base, M_{FC} = 100%) and the previous result for a floodplain with the angle of incidence between 7.5° and 9.3°. The resolution of the present result (72 m x 72 m) is close to the 100-m resolution of the previous result; however, the accuracy is less than that for the 100-m resolution case.

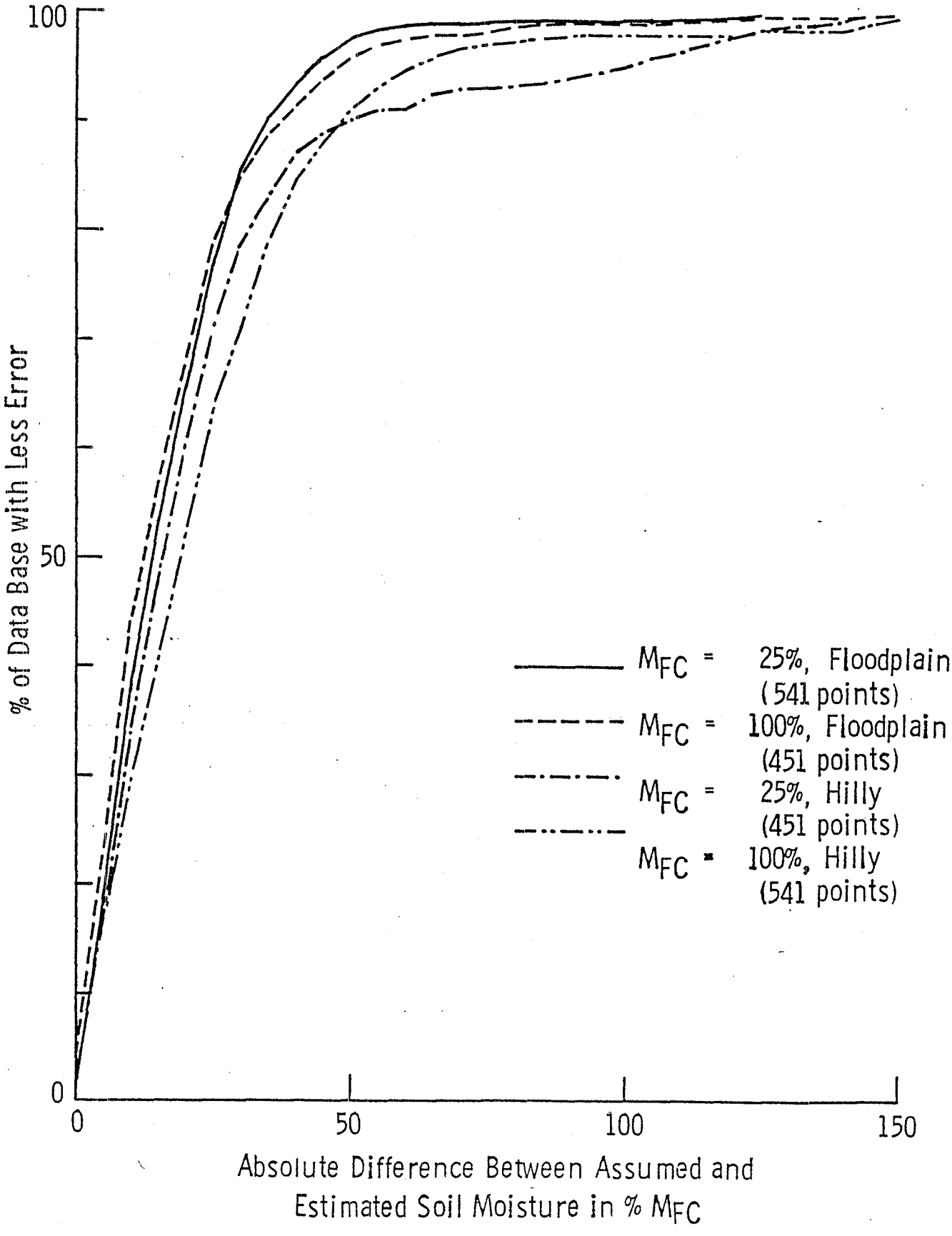

Fig. 24. Cumulative distributions of the absolute difference between assumed and estimated M_{FC}.

TABLE 11

Summary of the Estimation Error of Soil Moisture. Estimations are Made by the Algorithms Corresponding to the Target, i.e., Bare Soil or Vegetation-Covered Soil.

Absolute Value of Estimation Error	Floodplain		Hilly	
	Assumed M_{FC}		Assumed M_{FC}	
	25%	100%	25%	100%
0	2.0	3.3	1.7	2.6
5	18.5	23.1	18.4	18.0
10	37.9	44.1	34.0	29.7
15	53.5	57.2	48.0	41.0
20	65.7	68.1	60.0	52.1
25	76.8	78.7	71.2	64.0
30	85.5	85.1	78.8	71.2
35	90.4	88.9	83.1	79.0
40	93.3	91.4	86.8	84.6
45	96.2	93.8	88.8	88.3
50	97.6	96.0	90.1	91.1
55	98.4	97.1	90.9	93.3
60	98.7	97.6	91.1	94.8

In order to take these differences into account, we will examine the following two points. First, in the present simulation study, coherent processing of the SAR is completely included, so that the power received through the sidelobes may affect the performance of the SAR in its ability to detect soil moisture. To examine this point, simplified computer simulations are made in which the beamwidth of the SAR is assumed to have the value that is attained by coherent processing in the absence of sidelobes. This situation is the same as the one in the previously cited work (Ulaby et al., 1981). Some percentage values for the specific error of the soil moisture estimation are listed in Table 12, along with the values for the SAR, using coherent processing. As seen in the table, there are no significant differences between a SAR with sidelobes and a SAR without sidelobes at an estimation error of 20%, except for the hilly data base when M_{FC} = 25%. Therefore, we cannot attribute the cause of the differences in estimation error to the effect of the sidelobes. The second point is that the generalized estimation algorithm for soil moisture is based on experimental data for some target categories, and these contributions to the algorithm are almost even with each other. In the actual data base, however, the percentages of area for each target category are weighted in a specific manner, so that the estimation by the generalized algorithm may introduce an estimation bias that may degrade the accuracy of the soil moisture estimation. The estimation algorithms are tailored by taking into account the percentage of area of each target category, and are applied to soil moisture estimation. The results are shown in Table 13 along with the results obtained with the generalized algorithm. Again, there are no clear improvements in estimation accuracy, so the

TABLE 12

Accuracy Comparison of Soil Moisture Estimation
for a SAR With and Without Sidelobes

Absolute Value of Estimation Error	Floodplain				Hilly			
	Assumed M_{FC}				Assumed M_{FC}			
	25%		100%		25%		100%	
	With Sidelobes	Without Sidelobes	With Sidelobes	Without Sidelobes	With Sidelobes	Without Sidelobes	With Sidelobes	Without Sidelobes
0	1.9	1.1	2.1	1.4	1.2	2.7	1.3	0.3
5	17.1	17.4	18.7	19.4	17.3	20.0	15.5	15.2
10	31.5	33.9	33.4	36.5	30.8	36.3	28.3	27.5
15	47.7	50.1	46.1	49.6	44.0	52.2	39.5	40.7
20	62.1	63.4	58.2	59.5	54.8	62.7	52.3	51.3
25	70.9	75.2	66.1	68.0	64.5	70.7	61.0	61.5
30	79.4	83.5	71.7	74.6	73.5	76.2	67.7	70.2
35	85.3	88.3	76.2	78.6	77.8	79.5	76.5	75.0
40	89.9	91.7	80.2	83.5	82.7	83.0	82.3	80.8
45	93.4	93.8	84.0	86.1	85.3	84.7	87.0	86.3
50	95.4	94.9	87.2	88.2	86.2	86.5	90.2	89.0
55	96.3	96.0	89.4	88.8	87.2	87.3	92.5	91.8
60	97.8	96.6	90.9	89.3	87.8	88.3	93.8	94.5

TABLE 13

Accuracy Comparison of Soil Moisture Estimation by Means of a Generalized and a Tailored Algorithm

Absolute Value of Estimation Error	Floodplain				Hilly			
	Assumed M_{FC}				Assumed M_{FC}			
	25%		100%		25%		100%	
	Generalized Algorithm	Tailored Algorithm	Generalized Algorithm	Tailored Algorithm	Generalized Algorithm	Tailored Algorithm	Generalized Algorithm	Tailored Algorithm
0	1.9	1.4	2.1	1.6	1.2	1.8	1.3	1.0
5	17.1	16.6	18.7	17.3	17.3	18.5	15.5	17.0
10	31.5	32.2	33.4	31.7	30.8	31.3	28.3	29.5
15	47.7	46.1	46.1	44.2	44.0	43.5	39.5	40.2
20	62.1	59.8	58.2	54.6	54.8	55.2	52.3	52.0
25	70.9	70.2	66.1	63.4	64.5	65.2	61.0	60.3
30	79.4	78.2	71.7	70.1	73.5	73.6	67.7	67.7
35	85.3	83.0	76.2	73.8	77.8	78.7	76.5	75.5
40	89.9	87.2	80.2	77.9	82.7	81.8	82.3	82.5
45	93.4	91.0	84.0	81.3	85.3	85.0	87.0	86.8
50	95.4	93.4	87.2	84.8	86.2	86.2	90.2	90.0
55	96.3	95.2	89.4	87.8	87.2	87.0	92.5	91.8
60	97.8	96.5	90.9	89.8	87.8	87.7	93.8	94.0

main cause of the difference between the present and the previous results (Ulaby et al., 1981) cannot be attributed to the difference in the distribution of target categories.

Summarizing the above, the inferiority of the present results with regard to soil-moisture estimation accuracy as compared to the previous results may be due to the effect of fading, since the previous work employed 23-look averaging while only four-look averaging was employed in the present study. To improve the accuracy of the soil moisture estimation, the number of samples used in the noncoherent averaging should be increased.

5.0 SUMMARY AND CONCLUSIONS

The ability of a spaceborne SAR to detect soil moisture was evaluated by means of a computer simulation technique. In the present simulation, coherent processing of a SAR is included except for the transient effect in the receiver. This means that the receiver has a sufficiently wide bandwith so that the signal from a certain range bin does not affect the signals in the following range bins. The SAR model adopted has a range-sequential processor, the main portion of which can be replaced by hardware implementations in order to reduce the amount of telemetry involved.

After developing the simulation package, it is applied to the actual data bases to evaluate the ability of a SAR to estimate soil moisture. The data bases represent a floodplain and a hilly area, in order to compare the effect of surface elevation. Two soil-moisture conditions, M_{FC} = 25% and M_{FC} = 100% are compared, representing dry and wet conditions, respectively.

The results, using a blind classifier, indicate that the estimation accuracy for the floodplain data base, where surface elevation is not so pronounced, is, as expected, higher than that for the hilly data base. The inferiority of the results for the hilly data base may be due to the effects of foreshortening and range-creep, along with the variation of the backscattering coefficient resulting from the surface elevation.

To examine the causes of estimation error, the results of computer simulations of the SAR, including coherent processing, are first compared with those of the idealized SAR in which there are no sidelobes. There exist no significant differences between the two, so the power received through the sidelobes does not play a significant role in performance degradation. Subsequently, soil moisture estimation is made by means of an algorithm that is tailored to match the data bases by accounting for the percentages of the areas of each target category. The results of a comparison between the estimation algorithms again do not show significant differences. The main cause of degradation in the estimation error of the present results, as compared with the previous results (Ulaby et al., 1981) can, therefore, be considered to be due to the smaller number of noncoherent averaging used in the present study.

Using the generalized estimation algorithm, estimation accuracies of 62% (floodplain data base, M_{FC} = 25%) and 52% (hilly data base, M_{FC} = 100%) are obtained within ±20% of soil moisture. Estimation accuracies of about 80% to 90% are obtained for ±40% soil moisture. These accuracies indicate the promising role of SARs for use in future systems utilizing spaceborne soil moisture estimators. However, to improve the accuracy of soil moisture estimation, a much larger number of pixels should be averaged to reduce the effect of fading.

REFERENCES

Dobson, M. C. and F. T. Ulaby (1981), "Microwave Backscatter Dependence on Surface Roughness, Soil Moisture, and Soil Texture: Part III - Soil Tension," *IEEE Trans. Geosci. Rem. Sensing,* GE-19, No. 1, pp. 51-61, January.

Holtzman, J. C., V. H. Kaupp, J. L. Abbott, V. S. Frost, E. E. Komp, and E. C. Davison (1977), "Radar Image Simulation: Validation of the Point Scattering Model, Volume I," RSL Technical Report 319-27, University of Kansas Center for Research, Inc., Lawrence, Kansas, June.

Meier, R. (1981), "Simulation of the Topographic Influence on SLAR Data for Soil Moisture Detection in a Hilly Area," *Rem. Sens. Environ.*, No. 11, pp. 245-251, November.

Moore, R. K., J. P. Claassen, E. Erickson, R.K.T. Fong, M. Komen, J. McCauley, S. McMillan, and S. K. Parashar (1977), "Radar Systems for a Polar Mission Final Report," RSL Technical Report 291-2, Vol. 1, University of Kansas Center for Research, Inc., Lawrence, Kansas, February.

Ulaby, F. T., P. P. Batlivala, and M. C. Dobson (1978), "Microwave Backscatter Dependence on Surface Roughness, Soil Moisture, and Soil Texture: Part I - Bare Soil," *IEEE Trans. Geosci. Electron.*, GE-16, No. 4, pp. 286-295, October.

Ulaby, F. T., G. A. Bradley, and M. C. Dobson (1979), "Microwave Backscatter Dependence on Surface Roughness, Soil Moisture, and Soil Texture: Part II - Vegetation-Covered Soil," *IEEE Trans. Geosci. Electron.*, GE-17, No. 2, pp. 33-40, April.

Ulaby, F. T., M. C. Dobson, J. A. Stiles, R. K. Moore, and J. C. Holtzman (1981), "Evaluation of the Soil Moisture Prediction Accuracy of a Space Radar Using Simulation Techniques," RSL Technical Report 429-1, University of Kansas Center for Research, Inc., Lawrence, Kansas, May.

Ulaby, F. T., R. K. Moore, and A. K. Fung (1982), *Microwave Remote Sensing: Active and Passive,* Volume 2: *Radar Remote Sensing and Surface Scattering and Emission Theory,* Addison-Wesley Publishing Co., Reading, Massachusetts, May.

The following material refers to the development of a simulation package without specifying the locations:

Beckner, F. L. and G. L. Crow (1977), "Definition of a Mathematical Model for an Orbiting Imaging Radar," ARL-TR-77-6, Applied Research Labs., University of Texas at Austin, January.

APPENDIX

In this appendix, program listings along with brief explanations for each are provided. The present simulation package consists of one main program and nine subroutines. Table A1 shows the names of the programs and their principal functions. The explanations of each program are given below.

Main Program

In this program, the definition of some constants, computations of current time and position of the SAR, computations of slant range for each cell, accumulations of data into the appropriate range bins, simulation of fading, etc., are made. First, the range-bin reference R(I) is computed to make the range bins correspond exactly to the data-base cells having a 36-m x 36-m resolution. This allows us to compare the SAR images directly with the data base itself.

The temporal progress of the simulations is governed by the pulse transmission, NPULSE. The current position of the SAR (RX) is computed at the time of pulse transmission. The slant range XYRNGE is calculated for each data-base cell at the time. The data-base data (surface elevation, soil texture, and target category) are condensed into one word representing each cell. By using the subroutine UNPACK, the contents are "unpacked" into three words for computation. By use of the subroutine ANGLE, the local angles of incidence for each data-base cell are computed. Backscattering coefficients for each data base are computed using the subroutine SCATCF by accounting for the local angle of incidence and the assumed soil moisture M_{FC}. After computing the backscattered powers by means of the radar equation (subroutine RADREQ),

the data are arranged so that the appropriate range bins can form a train of received echoes (video signal) for one transmitted pulse in the in-phase and quadrature form (VDOR and VDOI). These are then introduced into the subroutine for coherent processing (called SARPR) along with the current time.

After computing the received powers for each resolution cell, random numbers having Gaussian statistics of zero mean and unit standard deviation are added by the system function RMS to simulate the fading effect. Then, received powers for four resolution cells (two in the along-track and two in the across-track direction) are averaged to give the final simulated received power RPOWER for a resolution cell of 72 m x 72 m. The results are submitted to the subroutine MFCEST to estimate the soil moisture of the resolution cell.

TABLE A1

Names of Programs and Their Principal Functions

Program Name	Function
Main Program	To control the program flow. Formation of video signals in in-phase and quadrature components. Addition of fading. Providing four-look processor. Output control.
Subroutine DBASE	To read data from the computer file.
Subroutine AZOFF	To prepare reference oscillators to shift the video spectrum.
Subroutine UNPACK	To recover the data for surface elevation and target category from a one-word expression of the data for each data-base cell.
Subroutine GEOMET	To compute the mean elevation, inclinations in the along- and across-track directions, and the effective area.
Subroutine ANGLE	To compute the local angle of incidence.
Subroutine SCATCF	To compute the backscattering coefficient for the target canopy accounting for the soil moisture and the local angle of incidence.
Subroutine RADREQ	To compute the backscattered power for each data-base cell.
Subroutine SARPR	To accumulate the video signal to form the image of the target area. To compensate the Doppler frequency shifts for 50 resolution cells.
Subroutine MFCEST	To estimate the soil moisture from the simulated backscattered power.

MAIN PROGRAM

```
      DIMENSION VDOR(50),VDOI(50),R(51)
      COMMON/PRCR/RMAPR(50,50),RMAPI(50,50),PAI2
      COMMON/DB/IDBASE(51,51)
      COMMON/PRO/FOFF(50)
      PAI2=6.283185307
      DUM=31.66668
C           MFC IS ASSUMED TO BE 100%
      MFC=100
C           FACTOR FOR DEGREE TO RADIAN CONVERSION
      DETORD=0.017453292
C           FACTOR FOR RADIAN TO DEGREE CONVERSION
      RDTODE=57.29577951
      DO 51 IAZ=1,50
      DO 50 IRNGE=1,50
      RMAPR(IAZ,IRNGE)=0.
      RMAPI(IAZ,IRNGE)=0.
   50 CONTINUE
   51 CONTINUE
      CALL DBASE
      CALL AZOFF
      DO 53 I=1,51
      D=3.6E11+(78991.5+FLOAT(I-26)*36.)**2
      R(I)=SQRT(D)
   53 CONTINUE
      DO 100 NPULSE=1,508
      DO 52 IRNGE=1,50
      VDOR(IRNGE)=0.
      VDOI(IRNGE)=0.
   52 CONTINUE
      TIME=FLOAT(NPULSE-1)/3600.
      RX=TIME*7545.-531.29375
      DO 200 IRNGE=1,50
      YRNGE=78991.5+(FLOAT(IRNGE)-25.5)*36.
      DO 300 IAZ=1,50
      CALL UNPACK(IDBASE(IAZ,IRNGE),IEL11,ICAT)
      CALL UNPACK(IDBASE(IAZ+1,IRNGE),IEL21,IDUM)
      CALL UNPACK(IDBASE(IAZ,IRNGE+1),IEL12,IDUM)
      CALL UNPACK(IDBASE(IAZ+1,IRNGE+1),IEL22,IDUM)
      CALL GEOMET(IEL11,IEL21,IEL12,IEL22,EL,
     &                  ALPHA,BETA,AREA)
      EL=(EL-815.)*0.3048
      RH=600.E3-EL
C
      XRNGE=RX-(FLOAT(IAZ)-25.5)*36.
      XYRNGE=SQRT(XRNGE*XRNGE+YRNGE*YRNGE)
      THETA=ATAN(XYRNGE/RH)
      CALL ANGLE(THETA,ALPHA,BETA,THETAL)
      CALL SCATCF(ICAT,THETAL,MFC,SIGMA)
      IF(ICAT.EQ.99)GO TO 307
      RR=SQRT(RH*RH+YRNGE*YRNGE)
      DIST=RR+0.5*XRNGE*XRNGE/RR
      IF(DIST.LT.R(1))GO TO 300
      DO 250 ITEST=2,51
      IF(DIST.GE.R(ITEST))GO TO 250
      IBIN=ITEST-1
      GO TO 260
```

```
      250 CONTINUE
      260 CONTINUE
          PHASE=DIST*DUM
          IP=IFIX(PHASE)
          PHASE=(PHASE-FLOAT(IP))*PAI2
          CALL RADREQ(XRNGE,YRNGE,RH,AREA,SIGMA,AMP)
          VDOR(IBIN)=VDOR(IBIN)+AMP*COS(PHASE)
          VDOI(IBIN)=VDOI(IBIN)+AMP*SIN(PHASE)
      300 CONTINUE
C             END OF AZ LOOP
      200 CONTINUE
          CALL SARPR(TIME,VDOR,VDOI)
C
      100 CONTINUE
          ISD=1218
          ISD=ISEED(ISD)
          DO 501 I=1,50
          DO 500 J=1,50
          PWR=RMAPR(I,J)**2+RMAPI(I,J)**2
          PWR=SQRT(PWR*0.5)
          RMAPR(I,J)=(RMS(ISD)*PWR)**2+(RMS(ISD)*PWR)**2
      500 CONTINUE
      501 CONTINUE
          DO 503 I=1,25
          DO 502 J=1,25
          RPOWER=(RMAPR(I*2-1,J*2-1)+RMAPR(I*2,J*2-1)
     &           +RMAPR(I*2-1,J*2)+RMAPR(I*2,J*2))*0.25
          RMAPR(I,J)=SQRT(RPOWER)
      502 CONTINUE
      503 CONTINUE
          DO 506 IRNGE=1,25
          Y=78991.5+FLOAT(IRNGE-13)*72.
          THETAE=ATAN(Y/600.E3)*RDTODE
          DO 505 IAZ=1,25
          CALL MFCEST(RMAPR(IAZ,IRNGE),THETAE,TOT,BAR,VEG)
          WRITE(6,504)IAZ,IRNGE,TOT,BAR,VEG
      504 FORMAT(' ',2(I2,2X),3(5X,F8.1))
      505 CONTINUE
      506 CONTINUE
          GO TO 821
      307 WRITE(6,308)
      308 FORMAT(1H ,10HSCATCF ERR)
      821 STOP
          END
```

Subroutine DBASE

This subroutine reads the data-base data from the computer file and stores them into the array IDBASE. The original data in the file are at an interval of 18 m in both the along- and across-track directions. The designated value of the data interval for the simulations is 36 m for both directions, so that the data are transferred alternately from the file to the IDBASE array. The dimensions of IDBASE are (51, 51) to accommodate the elevation data for computation of 2500 mean elevations.

Subroutine DBASE

```
      C
            SUBROUTINE DBASE
      C           ASSUMED DATA BASE ELEMENT IS 36M BY 36M
            COMMON/DB/IDBASE(51,51)
            DIMENSION JDBASE(102)
      C
            DO 103 I=1,101
      C           READ DATA BASE DATA FROM A FILE WITH 18M RES
            READ(01,101)(JDBASE(J),J=1,102)
        101 FORMAT(8(I8,1X))
            IF(MOD(I,2).EQ.0)GO TO 103
            IAZ=(I-1)/2+1
            DO 102 K=1,101
            IF(MOD(K,2).EQ.0)GO TO 102
            IRNGE=(K-1)/2+1
            IDBASE(IAZ,IRNGE)=JDBASE(K)
        102 CONTINUE
        103 CONTINUE
            RETURN
            END
```

Subroutine AZOFF

This subroutine provides us with the reference-oscillator signals used to shift the spectrum of the SAR video signal. The frequency difference between two adjacent oscillators is DOPCEL (14.2128638 Hz) which corresponds to the difference in the Doppler frequency shift at the two points with an interval of 36 m in the along-track direction. DOPCEL is calculated by the following equation:

$$\text{DOPCEL} = \frac{2ur_a}{\lambda R} , \qquad (A.1)$$

where u is the speed of the spacecraft; r_a is the resolution, which is 36 m; λ is the wavelength of 6.316×10^{-2} m; and R is the distance between the SAR and the target. The number of reference oscillators, FOFF, is 50, to provide 50 resolution cells.

Subroutine AZOFF

```
1       C
2             SUBROUTINE AZOFF
3             COMMON/PRO/FOFF(50)
4             DOPCEL=14.2128638
5             DO 100 IAZ=1,50
6             FOFF(IAZ)=DOPCEL*(FLOAT(IAZ)-25.5)
7           100 CONTINUE
8             RETURN
9             END
```

Subroutine UNPACK

Data for the three parameters, which are surface elevation, soil texture, and target category, are packed into one word, IDATA, in order to reduce computer-memory usage. This subroutine recovers the values of the surface elevation IEL and the information of the target category ICAT by using bit manipulations. A soil-texture extraction is not included in this subroutine, since the information is not used in the present simulation.

Subroutine UNPACK

```
      C
            SUBROUTINE UNPACK(IDATA,IEL,ICAT)
            INTEGER CATMSK
            DATA CATMSK/077/
            IEL=FLD(18,12,IDATA)
      C           ELEVATION IS MEASURED IN FEET
            ICAT=AND(IDATA,CATMSK)
      C           ICAT MEANS A CATEGORY OF TARGETS
            RETURN
            END
```

Subroutine GEOMET

One of the factors that should be accounted for in radar simulation studies is the topography of the target area. By using the surface elevation data at the four corners of the square data-base cell, the mean elevation, the inclination angles of the data-base cell in the along- and across-track directions, and the effective area of the data-base cell are all computed in this subroutine.

The mean elevation EL is given by averaging the four elevations at the four corners of the data-base cell. The surface inclinations ALPHA and BETA in the along- and across-track directions are calculated by computing the difference between two averaged elevations, which are derived by averaging two elevations in the across-track direction for ALPHA and in the along-track direction for BETA, at a distance of 36 m (236.2204724 feet) as,

```
A=FLOAT(I12+I22-I11-I21)/236.2204724
ALPHA=ATAN(A)                                          (A.2)
B=FLOAT(I21+I22-I11-I12)/236.2204724
BETA=ATAN(B).                                          (A.3)
```

The effective area AREA normalized by the assumed 36-m x 36-m area is computed by accounting for the surface inclinations as,

```
AREA=1/COS(ALPHA)/COS(BETA).                           (A.4)
```

Subroutine GEOMET

```
      C
            SUBROUTINE GEOMET(I11,I21,I12,I22,EL,ALPHA,BETA,AREA)
            EL=FLOAT(I11+I21+I12+I22)*0.25
      C
            A=FLOAT(I12+I22-I11-I21)/236.2204724
            ALPHA=ATAN(A)
      C
            B=FLOAT(I21+I22-I11-I12)/236.2204724
            BETA=ATAN(B)
      C
            AREA=1./COS(ALPHA)/COS(BETA)
            RETURN
            END
```

Subroutine ANGLE

This subroutine computes the local angle of incidence THETAL by accounting for the inclination of the data-base cell (ALPHA and BETA) along with the angle of incidence for the flat surface (THETA). The formula is as follows:

$$\text{THETAL}=\text{ARCOS}\ \frac{\text{TAN(BETA)*SIN(THETA)+COS(THETA)}}{\text{SQRT(TAN(ALPHA)**2+TAN(BETA)**2+1)}}\ . \qquad \text{(A.5)}$$

Subroutine ANGLE

```
1       C
2             SUBROUTINE ANGLE(THETA,ALPHA,BETA,THETAL)
3       C           THIS SUBROUTINE CALCULATES A LOCAL INCIDENT ANGLE
4             A=TAN(BETA)*SIN(THETA)+COS(THETA)
5             B=SQRT(TAN(ALPHA)**2+TAN(BETA)**2+1.)
6             THETAL=ARCOS(A/B)
7             RETURN
8             END
```

Subroutine SCATCF

The backscattering coefficient σ^{o} is calculated using the empirically determined algorithm based on the experimental data. For bare soils and vegetation-covered soils, the general form of the algorithm is shown below:

```
SIGMA = F + G * MFC                                    (A.6)
```

with

```
F=F1+F2*THETA+F3*THETA**2+F4*THETA**3                  (A.7)

G=G1+G2*THETA+G3*THETA**2+G4*THETA**3,                 (A.8)
```

where MFC is the soil moisture and THETA is the local angle of incidence. The coefficients Fi (i=1,..,4) and Gi (i=1,..,4) are listed in Table 6 in the text.

The backscattering coefficients for railroads, highways, bridges, and buildings where no water content can be defined are assumed to have a constant value of 10 dB independent of the local angle of incidence, therefore, F=10 and G=0. For trees and water bodies (lakes and rivers), again no water content can be defined, and the backscattering coefficients are assumed to be only a function of the local angle of incidence as follows:

Trees

```
F=10*ALOG10(10**-1.143*cos(THETA))                     (A.9)

G=0                                                    (A.10)
```

Water Bodies

```
F=22.82-5.126*THETA+0.237*THETA**2+3.973E-3*THETA**3   (A.11)

G=0                                                    (A.12)
```

F and G are substituted into Eq. A.6 together with the soil moisture MFC to determine the backscattering coefficient SIGMAO. The target category is specified through the value of index ICAT. The correspondence between ICAT and the target category is listed in Table A2.

TABLE A2

Correspondence Between the Index ICAT and the Target Category

ICAT	Target Category
3	Rough bare soil
4	Medium-rough bare soil
6	Railroads, highways, bridges, and buildings
7	Smooth bare soil and mown pasture
8	Pasture, alfalfa, and wheat
10	Trees
15	Soybeans E/W
16	Soybeans N/S
17	Milo E/W
18	Milo N/S
19	Corn E/W
20	Corn N/S
22	Rivers and lakes

Subroutine SCATCF

```
      C
            SUBROUTINE SCATCF(ICAT,THETA,MFC,SIGMA)
            A=THETA*57.29577951
            GO TO (99,99,1,2,99,3,4,5,3,6,3,3,4,5,
     &              7,8,9,10,11,12,5,13,6,13),ICAT
         99 ICAT=99
            GO TO 200
      C
      C           ROUGH BARE SOIL
          1 F=-15.09+A*(0.219+A*(-2.25E-2+A*0.332E-3))
            G=0.157+A*(-0.353E-2+A*(0.191E-3-A*0.22E-5))
            GO TO 100
      C           MEDIUM GOUGH BARE SOIL
          2 F=-11.69+A*(-0.512+A*(1.52E-2-A*0.202E-3))
            G=0.137+A*(0.463E-2+A*(-0.381E-3+A*0.7E-5))
            GO TO 100
      C           RAIL ROAD, HIGHWAY, BRIDGE AND BUILDING
          3 F=10.
            G=0.
            GO TO 100
      C           MOWN PASTURE AND SMOOTH BARE SOIL
          4 F=-5.13+A*(-1.961+A*(8.59E-2-A*1.375E-3))
            G=0.182+A*(-0.122E-2+A*(-0.123E-3+A*0.287E-5))
            GO TO 100
      C           PASTURE, ALFALFA AND WHEAT
          5 F=-1.675+A*(-3.045+A*(19.8E-2-A*3.674E-3))
            G=0.107+A*(2.522E-2+A*(-2.523E-3+A*5.278E-5))
            GO TO 100
      C           TREE
          6 F=10.*ALOG10(10.**(-1.143)*COS(THETA))
            G=0.
            GO TO 100
      C           SOYBEAN E-W
          7 F=-10.+A*(-0.591+A*(2.81E-2-A*0.509E-3))
            G=0.181+A*(-0.614E-2+A*(0.041E-3+A*0.228E-5))
            GO TO 100
      C           SOYBEAN N-S
          8 F=-10.+A*(-0.574+A*(3.31E-2-A*0.676E-3))
            G=0.181+A*(-0.614E-2+A*(0.041E-3+A*0.228E-5))
            GO TO 100
      C           MILO E-W
          9 F=-9.74+A*(-0.311+A*(0.835E-2-A*0.108E-3))
            G=0.124+A*(-0.502E-2+A*(0.132E-3-A*0.113E-5))
            GO TO 100
      C           MILO N-S
         10 F=-9.74+A*(-0.294+A*(1.34E-2-A*0.275E-3))
            G=0.124+A*(-0.502E-2+A*(0.132E-3-A*0.113E-5))
            GO TO 100
      C           CORN E-W
         11 F=-7.77+A*(-0.369+A*(-0.036E-2+A*0.133E-3))
            G=0.128+A*(-0.093E-2+A*(-0.205E-3+A*0.607E-5))
            GO TO 100
      C           CORN N-S
         12 F=-7.77+A*(-0.352+A*(0.464E-2-A*0.034E-3))
            G=0.128+A*(-0.093E-2+A*(-0.205E-3+A*0.607E-5))
            GO TO 100
```

```
57        C
58        C               RIVER AND LAKE
59             13 F=22.82+A*(-5.126+A*(0.237-A*3.973E-3))
60                G=0.
61        C
62        C               SIGMA IS CALCULATED IN DB
63           100 SIGMA=F+G*FLOAT(MFC)
64        C
65        C               TRANSLATE INTO REAL VALUE
66        C
67                SIGMA=10.**(SIGMA*0.1)
68           200 RETURN
                 END
```

Subroutine RADREQ

The computations of the received powers are made by means of the radar equation, having the following form:

$$P = C * AREA * SIGMA / (X**2 + Y**2 + Z**2)**2, \qquad (A.13)$$

where P is the received power, AREA is the effective area, SIGMA is the backscattering coefficient, and X, Y, and Z are the distances between the radar and the target in each coordinate. C is a function of the transmitted power, antenna gain, and the wavelength of the radar signal; however, it is assumed to be the same as the value of R_o^4, where R_o is the distance between the spacecraft's trajectory and the center of the data base in order to prevent P from having an extreme value. In the estimation of soil moisture, this slight modification of the radar equation will be taken into account.

Subroutine RADREQ

```
1       C
2             SUBROUTINE RADREQ(X,Y,Z,AREA,SIGMA,AMP)
3             C=1.341314863E23
4       C        C IS A CONSTANT FOR SCALING AMP AS AN APPROP. VALUE
5             P=C/(X*X+Y*Y+Z*Z)**2*AREA*SIGMA
6             AMP=SQRT(P)
7             RETURN
8             END
```

Subroutine SARPR

This subroutine simulates the function of the comb-filter, which is the SAR processor itself, together with phase compensations to remove the effect of the Doppler frequency shift for the data-base center.

The amount of the Doppler frequency shift f_d is given as follows:

$$f_d = \frac{-2uX}{\lambda R} , \qquad (A.14)$$

where u is the speed of the spacecraft, X is the distance between the radar and the target in the along-track direction, λ is the wavelength of the radar signal, and R is the distance between the radar and the target. The phase of the Doppler frequency shift can be expressed as follows by substituting X = ut - x, where -x is the position of the radar at time t = 0.

$$P = - \frac{2\pi u^2 t^2}{\lambda R} + \frac{4\pi uxt}{\lambda R} . \qquad (A.15)$$

Substituting u = 7545, $\lambda = 6.3158 \times 10^{-2}$, $R = 605.177 \times 10^3$ and $\pi = 3.14159265$, the above equation is rewritten in the following form:

P = (-1489.389685*TIME+209.755714)*TIME. (A.16)

The frequency offsets needed to provide 50 resolution cells in the along-track direction are made by adding their phase terms as computed by FOFF*TIME, where FOFF is the reference frequency generated in the subroutine AZOFF and TIME is the current time. Phase compensations are performed for the in-phase (VDOR) and quadrature (VDOI) components of the radar video signal as,

$$DR = VDOR * CR - VDOI * CI \quad (A.17)$$

$$DI = VDOR * CI + VDOI * CR, \quad (A.18)$$

where DR and DI are the in-phase and quadrature components after phase compensations and CR and CI are given by the following equations:

$$CR = COS(P + FOFF * TIME) \quad (A.19)$$

$$CI = SIN(P + FOFF * TIME). \quad (A.20)$$

Subroutine SARPR

```
      C
            SUBROUTINE SARPR(TIME,VDOR,VDOI)
            DIMENSION VDOR(50),VDOI(50)
            COMMON/PRCR/RMAPR(50,50),RMAPI(50,50),PAI2
            COMMON/PRO/FOFF(50)
            P=(-1489.389685*TIME+209.755714)*TIME
            DO 100 IAZ=1,50
            PP=P+FOFF(IAZ)*TIME
            IP=IFIX(PP)
            PPP=(PP-FLOAT(IP))*PAI2
            CR=COS(PPP)
            CI=SIN(PPP)
            DO 200 IRNGE=1,50
            DR=VDOR(IRNGE)*CR-VDOI(IRNGE)*CI
            DI=VDOR(IRNGE)*CI+VDOI(IRNGE)*CR
            RMAPR(IAZ,IRNGE)=RMAPR(IAZ,IRNGE)+DR
            RMAPI(IAZ,IRNGE)=RMAPI(IAZ,IRNGE)+DI
      200   CONTINUE
      100   CONTINUE
            RETURN
            END
```

Subroutine MFCEST

In this subroutine, soil moisture is estimated in the form of percent M_{FC} from the simulation results. The backscattering coefficients simulated are first divided by 508, which is the number of pulses transmitted, and gives the coefficient for one-pulse transmission. It is translated into dB by adding the calibration factor, 1.671 dB, which is explained in Section 3.4 of the text as,

```
SIGMA = 20 * ALOG10(SIGMA) + 1.671.                    (A.21)
```

The estimation algorithms are then applied to the calibrated backscattering coefficients, along with the angle of incidence for a flat surface. Three algorithms are used, and consist of one for bare soil, one for vegetation-covered soil, and an amalgam of the two. The general form of the estimation algorithm is shown below:

$$\text{MFC} = \frac{\text{SIGMA+A1+A2*THETA+A3*THETA**2+A4*THETA**3}}{\text{B1+B2*THETA+B3*THETA**2+B4*THETA**3}} . \qquad (A.22)$$

The coefficients Ai (i=1,..,4) and Bi(i=1,..,4) are listed in Table 8 in the text for the above three target categories.

Subroutine MFCEST

```
      C
            SUBROUTINE MFCEST(AMP,THETA,TOT,BAR,VEG)
            SIGMA=AMP/508.
            SIGMA=20.*ALOG10(SIGMA)+1.671
            A1=SIGMA+9.67+THETA*(0.84+THETA*(-4.59E-2+THETA
     &         *8.27E-4))
            A2=0.161+THETA*(9.38E-4+THETA*(-4.97E-4
     &         +THETA*1.21E-5))
            TOT=A1/A2
            B1=SIGMA+10.92+THETA*(8.37E-1+THETA*(-4.06E-2
     &         +THETA*7.84E-4))
            B2=0.17+THETA*(6.02E-4+THETA*(-3.76E-4+THETA
     &         *1.E-5))
            BAR=B1/B2
            C1=SIGMA+9.38+THETA*(9.57E-1+THETA*(-6.34E-2
     &         +THETA*1.23E-3))
            C2=0.165+THETA*(4.E-3+THETA*(-9.47E-4+THETA*2.27E-5))
            VEG=C1/C2
            RETURN
            END
```

End of Document